



Heterogeneous electrocatalysts design for nitrogen reduction reaction under ambient conditions

Yuchi Wan¹, Jichu Xu¹, Ruitao Lv^{1,2,*}

¹ State Key Laboratory of New Ceramics and Fine Processing, School of Materials Science and Engineering, Tsinghua University, Beijing 100084, China

² Key Laboratory of Advanced Materials (MOE), School of Materials Science and Engineering, Tsinghua University, Beijing 100084, China

Ammonia, as an important carbon-free energy carrier and also an important chemical for producing fertilisers, is mainly synthesized by a traditional Haber–Bosch process with high energy consumption and large amounts of greenhouse gas emissions. Recently, electrocatalytic nitrogen reduction reaction (NRR) has attracted worldwide research attentions as a promising route for achieving green and sustainable ammonia synthesis at ambient conditions. Although exciting advances have been made in the NRR field, the development of electrochemical nitrogen-to-ammonia conversion is still challenging because of the low ammonia yield and unsatisfactory Faradaic efficiency mainly deriving from the poor catalytic activity of catalysts. Herein, various catalyst design strategies for increasing the exposed active sites or altering the electronic structure aiming at improving the apparent activity or intrinsic activity are summarized in this review article. On the basis of effective design strategies, a range of recently reported NRR electrocatalysts, including noble metal-based materials, non-noble metal-based materials, single-metal-atom catalysts, and metal-free materials, are summarized, and the mechanisms of tuning the catalytic activity by applying the design strategies are emphasized based on the combination of theoretical calculations and experimental investigations. It is anticipated that the established correlation between physicochemical properties of catalysts and NRR performance can provide guidance for designing heterogeneous NRR electrocatalysts with high activity, good selectivity, and high stability.

Introduction

Nitrogen (N_2) fixation via the conversion of atmospheric nitrogen to ammonia (NH_3) has been regarded as one of the significant processes in the industry, since ammonia not only plays a key role in producing fertilisers to sustain the rising global population but also serves as a green energy carrier and an alternative fuel [1–3]. Nowadays, the industrial ammonia is mainly synthesized by the traditional Haber–Bosch process using iron-based catalysts at a high pressure (150–200 atm) and high temperature (300–500 °C) [2]. This process is highly energy-consuming and accounts for more than 1% of the world's energy consumption

[4,5]. Apart from the energy input during the high temperature process, steam reformation to produce the required hydrogen is responsible for 3–5% of the world's natural gas consumption and releases large amounts of greenhouse gases into the atmosphere [6–8]. In this regard, it is imperative to develop a green, sustainable, and alternative process to synthesize ammonia employing renewable resources at ambient conditions.

In the biological system, nitrogen fixation occurs naturally catalyzed by the nitrogenase enzymes mainly containing iron-molybdenum cofactor (denoted as FeMo-co) [9–12]. Notably, nitrogenase enzymes operate under mild conditions (<40 °C, atmospheric pressure) relying on the significant energy input delivered by the obligatory hydrolysis of adenosine triphosphate (ATP) molecules [2]. Inspired by the biological nitrogen fixation,

* Corresponding author at: State Key Laboratory of New Ceramics and Fine Processing, School of Materials Science and Engineering, Tsinghua University, Beijing 100084, China.

E-mail address: Lv, R. (lrvuitao@tsinghua.edu.cn).

homogeneous (molecular) catalysts have been designed to reduce atmospheric nitrogen through multiple proton and electron transfer steps [13–15]. However, the poor stability of the nitrogenase enzymes and the molecular catalysts remains a big challenge, and detailed reaction mechanism deserves intensive investigation.

Recently, electrochemical and photochemical approaches using heterogeneous catalysts have attracted increasing attentions for achieving nitrogen reduction reaction (NRR), benefiting from the mild operating conditions and the utilization of renewable energy sources [16]. Nevertheless, photocatalytic nitrogen reduction is not as efficient as the electrocatalytic counterpart on account of low utilization of solar energy and easy recombination of charge carriers (electron–hole pairs) during the photochemical process [17]. In contrast, electrochemical catalysis can be facilely controlled by adjusting the potentials and reaction temperature to obtain the desired product [18]. Moreover, the electrocatalytic process using water as the sustainable proton source to substitute for the raw material hydrogen gas used in the Haber–Bosch process is feasible to lower the energy demand, decrease the emissions of CO₂, and simplify the reactor design [19,20].

In principle, electrochemical ammonia synthesis can take place at room temperature and atmospheric pressure, whereby the thermodynamic driving force is controlled by the applied voltage [21]. However, the electrocatalytic NRR process is suppressed by the slow kinetics of N₂ adsorption and the sluggish splitting of the strong N≡N bond, resulting in a large overpotential and low NH₃ yield [22]. In addition, it is challenging for electrocatalytic NRR that the competing hydrogen evolution reaction (HER) is always dominant in the electrochemical system, because theoretical limiting potential for the HER is smaller than that for the NRR according to the volcano plot constructed by Nørskov and coworkers [23]. From a kinetic perspective, most of the protons and electrons go toward the evolution of H₂ rather than the synthesis of NH₃, which accounts for the extremely low Faradaic efficiency (FE) of heterogeneous electrocatalysts for NRR at ambient conditions [24]. Therefore, it is of great significance to optimize the whole electrochemical system, including the reactor configuration, electrolyte, and electrocatalysts, in order to achieve low overpotential, high NH₃ yield, and high Faradaic efficiency, while suppressing the competing HER process. As the core components of the electrochemical system, heterogeneous electrocatalysts with high activity, high selectivity, and good stability are supposed to be elaborately developed to enable the electrocatalytic NRR at ambient conditions.

There are generally two strategies for electrocatalyst design with the purpose of improving the activity of the NRR electrocatalysts: (1) increasing the apparent activity and (2) promoting the intrinsic activity [25]. On the one hand, the apparent activity of electrocatalysts always depends on the number of exposed active sites, which is influenced by the crystal structure and extrinsic properties of materials, such as size and shape. Hence, the apparent activity can be tuned by the crystal facet regulation and morphology and size engineering, aiming at exposing more active sites and improving the utilization of active sites. On the other hand, the intrinsic activity is associated with the electronic structure of materials. Accordingly, the strain engineering and defect

engineering, including the vacancy modulation along with the heteroatom doping, could constitute powerful routes to tailor the electronic structure of the catalyst for achieving a high intrinsic activity of each active site. Nearly all the strategies mentioned above have been successfully applied in the design of heterogeneous electrocatalysts toward some intensively studied electrochemical reactions, including HER, oxygen evolution reaction (OER), oxygen reduction reaction (ORR), and carbon dioxide (CO₂) reduction; nevertheless, investigations on rational design of heterogeneous electrocatalysts for NRR are still relatively limited. Therefore, the systematic summarization of effective and facile strategies for material design is expected to inspire insights into the development of highly efficient heterogeneous electrocatalysts toward NRR. Based on the above strategies while combining theory and experiment, a series of electrocatalysts, including noble metal-based materials, non-noble metal-based materials, single-metal-atom catalysts, and metal-free materials, have been designed and/or synthesized for NRR at ambient conditions. Thus, systematic classification of recently developed NRR electrocatalysts and analysis of corresponding material design principles could open the avenue of rational design and selection of efficient NRR electrocatalysts.

This review article focuses on the rational design of heterogeneous electrocatalysts toward NRR for achieving low overpotential and high Faradaic efficiency, as well as high NH₃ yield. Firstly, fundamental reaction mechanisms of the electrocatalytic NRR are presented. Then the various strategies to improve the apparent activity or intrinsic activity of the NRR electrocatalysts are proposed. Considering that current review articles have already involved the previously developed NRR catalysts [3,16,19,26], we place emphasis on the state-of-the-art progress of this field and summarize recently explored NRR electrocatalysts classified by their chemical compositions, while discussing the effect of applied material design principles on their NRR performance. Finally, we provide some insights into the development of NRR electrocatalysts and summarize the remaining challenges and future directions in this emerging area.

Fundamental principles of electrocatalytic NRR

Reaction mechanisms of electrocatalytic NRR

Generally, the electrocatalytic nitrogen-to-ammonia conversion over a heterogeneous catalyst is based on two fundamental mechanisms, including dissociative and associative pathways, with different involved intermediates (Table 1). According to the dissociative mechanism (Fig. 1b), the adsorbed N₂ molecules firstly undergo the cleavage of the triple bond prior to the hydrogenation process with high energy input due to the inertness of N≡N bond, which can explain why harsh conditions are required for the Haber–Bosch process following the dissociative pathway. While in the associative pathway, the adsorbed N₂ molecule keeps two N atoms bound to each other before the formation of the first NH₃ molecule. Considering different sequences of the addition of H to the N atoms, the hydrogenation process in the associative mechanism can proceed via two ways, including the distal pathway and alternating pathway. In the distal pathway, the distal N atom far away from the end-on adsorption site preferentially undergoes the hydrogenation

TABLE 1**Mechanisms of the electrocatalytic NRR.**

Mechanism	Elementary reaction steps
Dissociative pathway	$\text{N}_2 + 2^* \rightarrow 2^*\text{N}$ $2^*\text{N} + 2\text{e}^- + 2\text{H}^+ \rightarrow 2^*\text{NH}$ $2^*\text{NH} + 2\text{e}^- + 2\text{H}^+ \rightarrow 2^*\text{NH}_2$ $2^*\text{NH}_2 + 2\text{e}^- + 2\text{H}^+ \rightarrow 2\text{NH}_3 + 2^*$
Associative distal pathway	$\text{N}_2 + * \rightarrow *^*\text{N}_2$ $*^*\text{N}_2 + \text{e}^- + \text{H}^+ \rightarrow *^*\text{NNH}$ $*^*\text{NNH} + \text{e}^- + \text{H}^+ \rightarrow *^*\text{NNH}_2$ $*^*\text{NNH}_2 + \text{e}^- + \text{H}^+ \rightarrow *^*\text{N} + \text{NH}_3$ $*^*\text{N} + \text{e}^- + \text{H}^+ \rightarrow *^*\text{NH}$ $*^*\text{NH} + \text{e}^- + \text{H}^+ \rightarrow *^*\text{NH}_2$ $*^*\text{NH}_2 + \text{e}^- + \text{H}^+ \rightarrow \text{NH}_3 + *$
Associative alternating pathway	$\text{N}_2 + * \rightarrow *^*\text{N}_2$ $*^*\text{N}_2 + \text{e}^- + \text{H}^+ \rightarrow *^*\text{NNH}$ $*^*\text{NNH} + \text{e}^- + \text{H}^+ \rightarrow *^*\text{NNH}_2$ $*^*\text{NNH}_2 + \text{e}^- + \text{H}^+ \rightarrow *^*\text{NHNH}_2$ $*^*\text{NHNH}_2 + \text{e}^- + \text{H}^+ \rightarrow *^*\text{NH}_2\text{NH}_2$ $*^*\text{NH}_2\text{NH}_2 + \text{e}^- + \text{H}^+ \rightarrow *^*\text{NH}_2 + \text{NH}_3$ $*^*\text{NH}_2 + \text{e}^- + \text{H}^+ \rightarrow \text{NH}_3 + *$

*Denotes an adsorption site on catalyst surface.

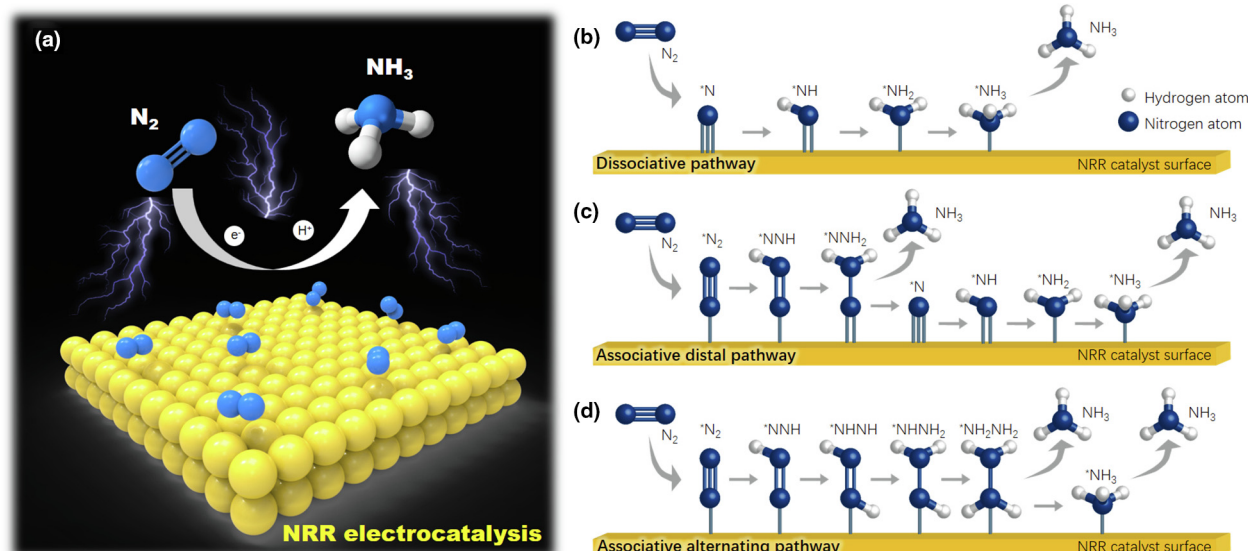
process until the release of the remote NH_3 molecule, and subsequently the remaining N adatom repeats the same hydrogenation process to produce the second NH_3 molecule (Fig. 1c). In comparison, the alternating pathway proceed with the two N atoms hydrogenated in turn accompanied by a proton-coupled electron transfer, and two NH_3 molecules are released sequentially at the final step of the pathway (Fig. 1d) [3,21]. In addition, the enzymatic pathway shares a similar hydrogenation process with the alternating pathway but with both N atoms binding to the catalyst surface following a side-on coordination mode, which doesn't usually occur on heterogeneous catalysts [19].

The fundamental mechanisms of electrochemical NRR have been further revealed by theoretical studies based on the calculations of the free energy changes of key intermediates in a specific

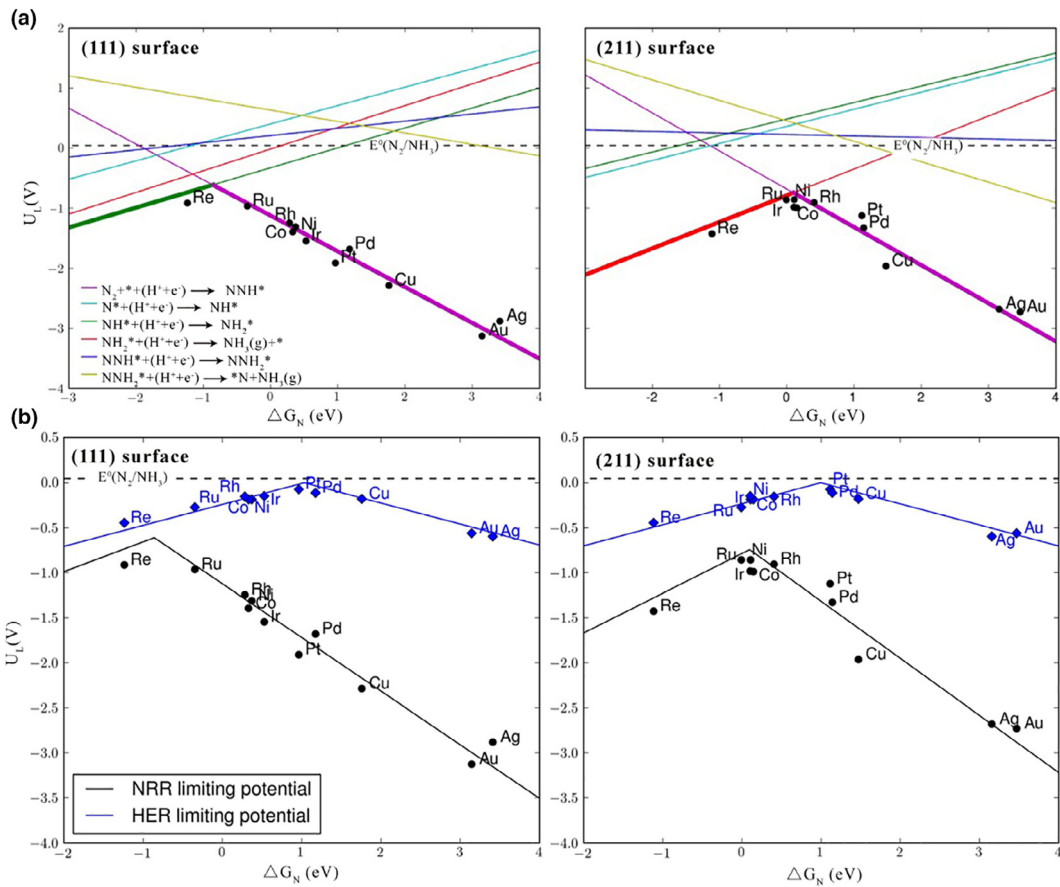
reaction step [23,27]. For instance, Nørskov's group constructed the correlation between the theoretical limiting potentials and the binding energies of N adatoms on various transition-metal surfaces [23]. Demonstrated by the density functional theory (DFT) calculations, the electrochemical nitrogen reduction is limited by the protonation of N_2 as $*^*\text{N}_2\text{H}$ for less reactive transition metals with weak nitrogen-binding capability, whereas the potential limiting step is the $*^*\text{NH}$ protonation to form $*^*\text{NH}_2$ or the desorption of $*^*\text{NH}_2$ as NH_3 for more-reactive transition metals binding nitrogen strongly (Fig. 2a). Therefore, a reduced overpotential can be obtained theoretically through the strong adsorption of $*^*\text{N}_2\text{H}$ on metals binding nitrogen weakly or selective destabilization of $*^*\text{NH}_2$ or $*^*\text{NH}$ on strong-binding metals. Metals, such as Re, Ru, and Rh, near the peak of the volcano plot possess appropriate nitrogen-binding capability. Nevertheless, even those metals exhibit large limiting potentials for nitrogen electroreduction that are at least 0.5 V more negative than the overpotential requirements of HER (Fig. 2b), indicating that the competing reaction HER is more favorable on most metal catalysts theoretically causing the unsatisfactory Faradaic efficiency for electrocatalytic ammonia synthesis. For this reason, more targeted strategies need to be implemented for the rational design of highly efficient NRR catalysts promoting the electrochemical nitrogen reduction to ammonia.

Research methods of electrocatalytic NRR**Electrochemical cell configurations**

The Electrochemical cell configuration is of extreme importance for performing electrochemical conversion of N_2 into NH_3 . The cell configurations applied in electrocatalytic NRR research mainly covered four types, including the back-to-back cell, the proton exchange membrane (PEM)-type cell, the single-chamber cell, and the "H"-type cell (Fig. 3) [19]. In the back-to-back cell (Fig. 3a), two gas-diffusion electrodes are usually separated by a proton exchange membrane or an anion exchange membrane,

**FIGURE 1**

Schematic illustrations of (a) the nitrogen reduction reaction (NRR) electrocatalysis and its possible mechanisms, including (b) dissociative pathway, (c) associative distal pathway, and (d) associative alternating pathway (Adapted from Ref. [21]).

**FIGURE 2**

(a) Limiting potentials for electrocatalytic nitrogen reduction reaction (NRR) as a function of *N binding energy on (111) surfaces and (211) surfaces of various transition metals. (b) Comparison of limiting-potential volcano plots of hydrogen evolution reaction (HER) (shown in blue) and NRR (shown in black) on (111) surfaces and (211) surfaces of various transition metals. Reproduced from Ref. [23] with permission from Wiley-VCH.

and the cathode and the anode are fed with N_2 gas and H_2O , respectively. Different from the back-to-back cell, the anode of the PEM-type cell (Fig. 3b) is filled with electrolyte solution, in which the water is electrolyzed to provide the protons for the cathode reaction. Both of the back-to-back cell and PEM-type cell own the potential for suppressing the HER by limiting the proton supply, whereas gas-solid reactions are mainly involved in the cathode chamber, which cannot be easily achieved at ambient conditions. As for the single-chamber cell (Fig. 3c), both the cathode reaction and the anode reaction occur in the same electrolyte solution, which might lead to the oxidation of produced ammonia at the anode causing the ammonia determination inaccurate. The most widely adopted reactor configuration under ambient condition is the "H"-type cell (Fig. 3d-f), in which the cathode reaction and the anode reaction are separated by a Nafion membrane. But the ammonia crossover effect can't be neglected, thus the ammonia content in both of the cathode electrolyte and anode electrolyte needs to be considered during the ammonia determination process.

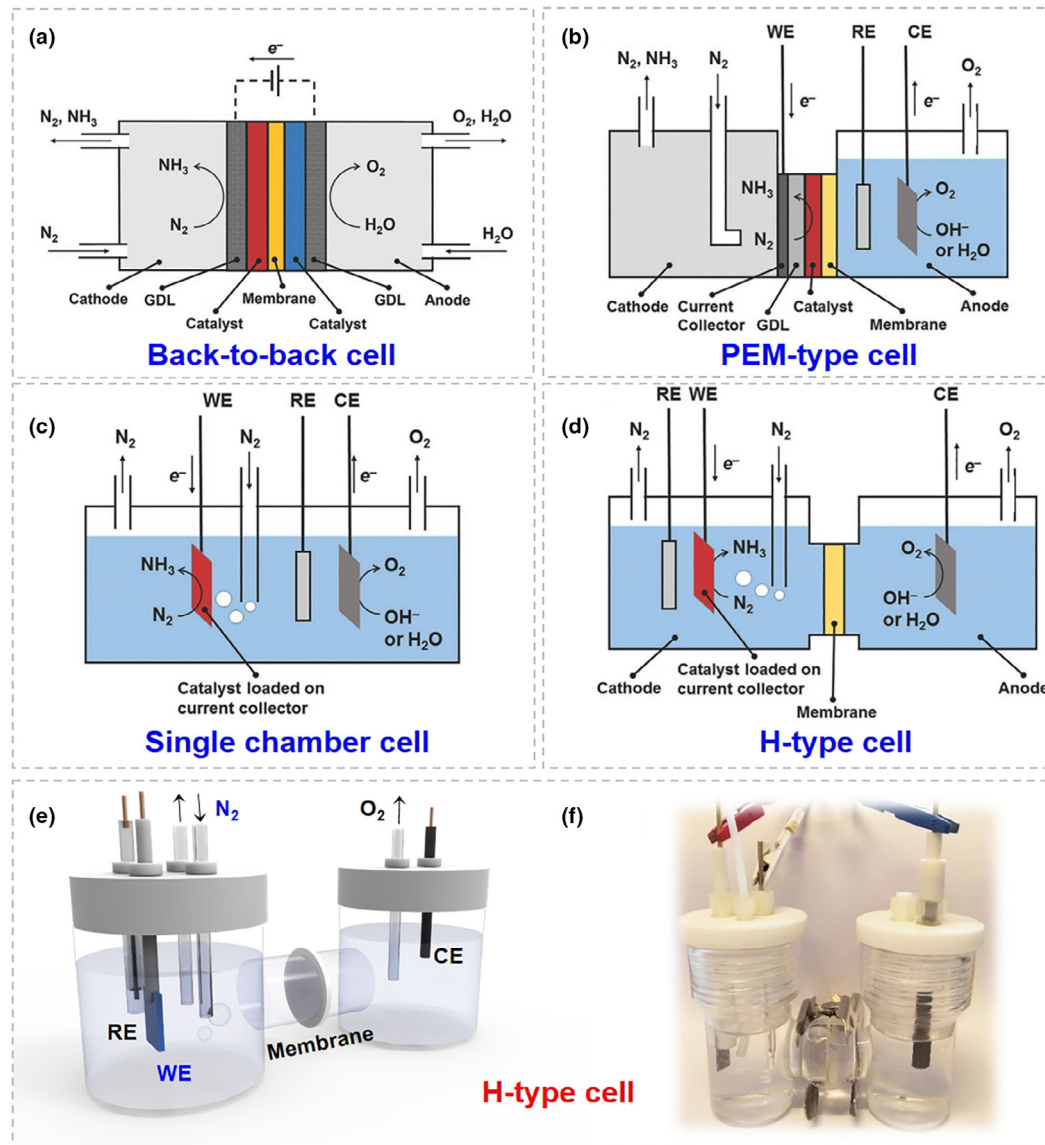
Electrochemical measurements

Electrochemical measurements for the electrocatalytic NRR usually involve the linear sweep voltammetry (LSV), chronoamperometry (CA), cyclic voltammetry (CV) and electrochemical

impedance spectroscopy (EIS). Linear sweep voltammetric curves depict the change of the current density across a potential range for the electrocatalytic NRR. By comparing the LSV curves measured in Ar-saturated or N_2 -saturated electrolyte, one can determine whether nitrogen reduction occurs at a certain potential range based on the difference of current density. As for the CA technique, the current is monitored as a function of reaction time at a controlled potential. As-obtained CA data can be used to calculate the Faradaic efficiency of NRR and to evaluate the stability of catalysts under long-term electrolysis. The stability of the electrochemical reaction system can be evaluated by the repetition of CV measurements. In addition, the CV technique can be used to determine the double-layer capacitance for estimating the electrochemically active surface area (ECSA), which can be used to normalize the surface area of the electrode by excluding the influence of surface roughness [28]. EIS measurements can be used to evaluate the reaction rate of NRR based on the determination of electrolyte resistance and charge-transfer resistance.

Ammonia detection

In order to accurately evaluate the catalytic activity of NRR catalysts, it is necessary to establish a reliable detection method for as-produced ammonia. The most common ammonia detection

**FIGURE 3**

Schematics of different electrochemical cell configurations, including (a) back-to-back cell, (b) PEM-type cell, (c) H-type cell, and (d) single-chamber cell. Here PEM denotes proton exchange membrane. Reproduced from Ref. [19] with permission from Wiley-VCH. (e-f) Schematic illustration and a photograph of an H-type cell, including WE (working electrode), RE (reference electrode), CE (counter electrode), and membrane.

method is the *colorimetric method*, including the *Nessler's reagent method* and the indophenol blue method, whereas the metallic ions or pH value of the solution might interfere with the NH₃ detection results. Therefore, the combination of colorimetric method and other methods like the ion-selective electrode analysis is essential to make the ammonia detection more convincing. In addition, ¹⁵N₂ isotopic experiments are required to identify the origin of the detected ammonia, especially for those NRR catalysts containing nitrogen species. Also, it is noteworthy that the ambient ammonia contamination might lead to erroneous results of the detected ammonia, especially when the ammonia yield is quite low. Accordingly, it is indispensable to conduct a series of rigorous control experiments, including the electrochemical Ar control experiments and the activity testing, in both Ar and N₂ under an open-circuit condition. With a

reasonable combination of multiple ammonia detection methods and a series of control experiments, the NRR performance of catalysts can be reliably evaluated to provide guidance for the future research.

Catalytic activity descriptors of electrocatalytic NRR

The *Faradaic efficiency* and the *NH₃ yield rate* are two important descriptors of the performance of an NRR electrocatalyst. The *Faradaic efficiency* can be defined as the ratio of the charge used for nitrogen reduction to the total charge passed through the circuit, which reflects the selectivity of the electrochemical process for NH₃ synthesis. The *NH₃ yield rate* refers to the NH₃ production per unit time and unit catalyst loading mass (or unit electrode surface area), which reflect the NRR reaction rate for NH₃ synthesis.

The Faradaic efficiency (η) of NRR can be calculated using Eq. (1), where n is the number of electrons required for producing one NH_3 molecule ($n = 3$), F is the Faraday constant ($F = 96485.33$), C is the measured NH_3 concentration, V is the volume of the electrolyte, M is the relative molecular mass of NH_3 ($M = 17$), and the Q is the total charge passed through the electrodes.

$$\eta = \frac{n \cdot F \cdot C \cdot V}{M \cdot Q} \quad (1)$$

The NH_3 yield rate (R) of NRR can be calculated using Eq. (2), where C is the measured NH_3 concentration, V is the volume of the electrolyte, t is the reaction time, and S is the catalyst loading mass or the geometric area of the electrode or the electrochemically active surface area of the electrode.

$$R = \frac{C \cdot V}{t \cdot S} \quad (2)$$

Design strategies for efficient NRR electrocatalysts

Currently, the development of electrocatalytic NRR at ambient conditions is obstructed by the high overpotential, low Faradaic efficiency, and low NH_3 yield. The effective method to overcome these obstacles is to design highly active and durable electrocatalysts for NRR. In the previous section, we have described material design principles aiming at improving the apparent activity or intrinsic activity of NRR electrocatalysts. In this section, we will discuss how the specific strategies, including the crystal facet regulation, the morphology and size engineering, the strain engineering, and the defect engineering, including creating vacancy and heteroatom doping, alter the number of active sites or the electronic structure and then tune the activity of NRR electrocatalysts. It is expected that the above strategies for the modification of catalytic activity can enlighten the intentional design of NRR electrocatalysts with excellent performance.

Strategies for increasing the apparent activity

Tuning the apparent activity of electrocatalysts is the most straightforward way to tailor the electrocatalytic behaviors. By rationally controlling the crystal facets, size, shape, and morphology of the catalytic materials, it is possible to create more active sites and maximize the exposure of active sites, which can lead to a remarkable improvement of electrocatalytic activity.

Crystal facet regulation

Rational regulation of crystal facets with favorable atomic arrangement and coordination provides an efficient strategy for maximizing the exposure of active sites and subsequently enhancing the electrocatalytic activity [29,30]. Moreover, the exposed crystal facets can influence the adsorption of electrolytes on the catalyst surface, thus affecting the catalytic performance [31,32]. For example, in strongly adsorbing electrolytes, such as sulfuric acid, the strong adsorption of sulfate anions on the (1 1 1) facets of single-crystal Pt can cause the active sites being blocked and lower the catalytic activity [30]. In addition to electrolytes, various exposed crystal facets can preferentially absorb different intermediates, which might affect the electrocatalytic selectivity [33–36].

For electrocatalytic ammonia synthesis, some breakthroughs have been made in selectively controlling the exposed crystal facets and subsequently boosting the apparent electrocatalytic activity. For example, the Mo nanofilm catalyst was reported to exhibit improved electrocatalytic activity toward NRR when increasing the ratio of (1 1 0) orientation in four plane orientations detected in X-ray diffraction (XRD) patterns, which achieved the highest NH_3 formation rate of 3.09×10^{-11} mol s $^{-1}$ cm $^{-2}$ and the highest Faradaic efficiency of 0.72% at -0.49 V vs RHE (reversible hydrogen electrode) [37]. However, only XRD patterns of the Mo nanofilm were provided, which were inadequate to identify the surface crystal facets of catalysts. By comparison, Yan's group utilized multiple characterization techniques, such as spherical aberration-corrected transmission electron microscope and ultraviolet-visible spectrum (UV-vis), to precisely identify the high-index {7 3 0} facets and surface atomic arrangements of obtained tetrahedral Au nanorods (Fig. 4) [38]. A maximum NH_3 production rate of $1.648 \mu\text{g h}^{-1}$ cm $^{-2}$ was achieved at -0.2 V vs RHE and the remarkably enhanced activity was attributed to the exposed stepped {7 3 0} facets, offering abundant active sites to capture and dissociate N_2 . However, the byproduct hydrazine hydrate ($\text{N}_2\text{H}_4 \cdot \text{H}_2\text{O}$) was detected, leading to the relatively poor selectivity of the catalysts. Furthermore, the NRR activity control experiments between different exposed surface facets are required to confirm the superior catalytic effect of stepped {7 3 0} facets.

Size and morphology engineering

Engineering the size and morphology of electrocatalysts is an effective strategy for optimizing their catalytic activities toward various electrochemical reactions [39]. The size of heterogeneous electrocatalysts can be tuned to create low-coordination sites apart from the original close-packed sites, which may influence the binding strength of reaction intermediates, thereby affecting the activity and selectivity of electrocatalysts [39,40]. In addition, morphology-controlled nanomaterials may have the optimal shape and/or nanostructure to provide large specific surface area along with high theoretical density of active sites that can facilitate the catalytic processes [41–43].

With regard to electrocatalytic NRR, morphology-controlled approach has been adopted in order to enhance the activity of electrocatalysts. Nazemi et al. reported hollow Au nanocages as an efficient NRR electrocatalyst, which achieved the highest ammonia Faradaic efficiency (30.2%) at -0.4 V vs RHE and significant ammonia yield ($3.9 \mu\text{g h}^{-1}$ cm $^{-2}$) at -0.5 V vs RHE at ambient conditions (Fig. 5e) [44]. As-prepared hollow Au nanocages exhibited superior NRR catalytic activity (Fig. 5f) compared with solid Au nanoparticles of various shapes, including nanocubes, nanospheres, and nanorods, with similar nanoparticle concentrations (Fig. 5a-d). The significant enhancement in the rate of electrocatalytic NRR using hollow Au nanocages was attributed to both the larger active surface area of the unique hollow structure leading to more exposed active sites and the confinement of the reactants inside the nanocage, which increased the residence time of N_2 molecules on the inner surface of nanocage, thus facilitating the conversion of N_2 to NH_3 . Furthermore, the same group investigated the effect of pore size/density and Ag content in the interior surface of hollow Au nanocages on

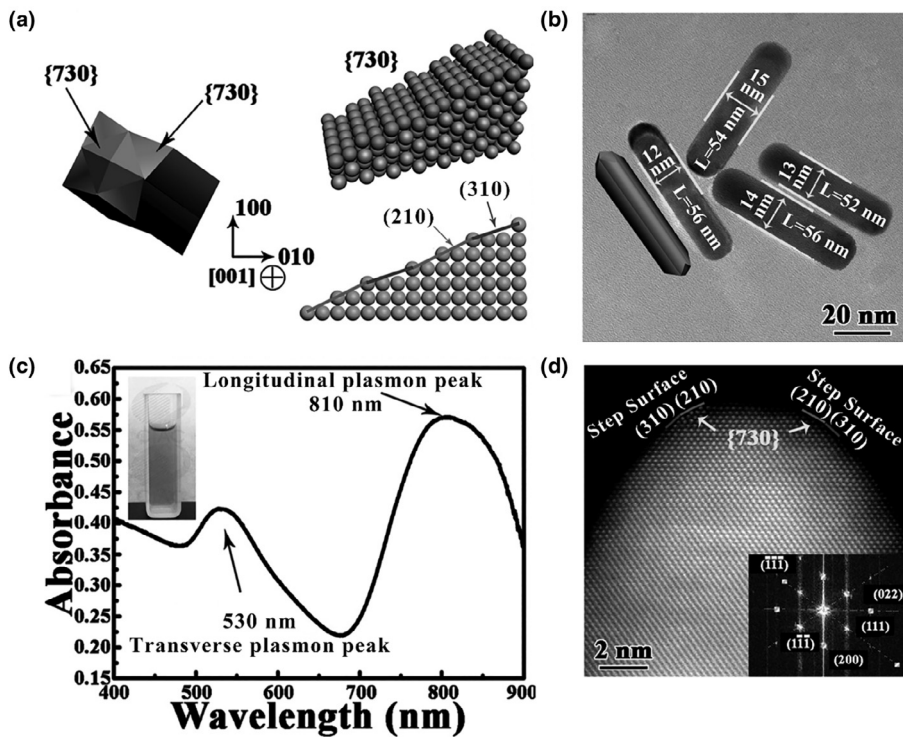


FIGURE 4

(a) Geometric models of an Au nanorod and exposed {730} facet composed of (210) and (310) sub-facets. (b) Transmission electron microscope (TEM) image of Au nanorods. (c) Ultraviolet-visible spectrum (UV-vis) extinction spectrum of the Au nanorods; the inset is the photograph of as-obtained Au nanorods suspended in water. (d) Spherical aberration corrected transmission electron microscope image of the Au nanorods with stepped sub-facets, the inset is the fast Fourier transform (FFT) pattern of the indicated region. Reproduced from Ref. [38] with permission from Wiley-VCH.

the electrocatalytic NRR activity by tuning their peak localized surface plasmon resonance from 635 to 795 nm [45]. It was found that the presence of Ag in the cavity decreased the electrocatalytic NRR activity of hollow Au nanocages due to the higher activity of Ag toward HER. Besides, increasing the pore size of the nanocage structure was unfavorable to the rise of NH₃ yield rate and Faradaic efficiency due to the decreased active surface area of the nanocages and inefficient confinement of N₂ molecules in the cavity.

Strategies for promoting the intrinsic activity

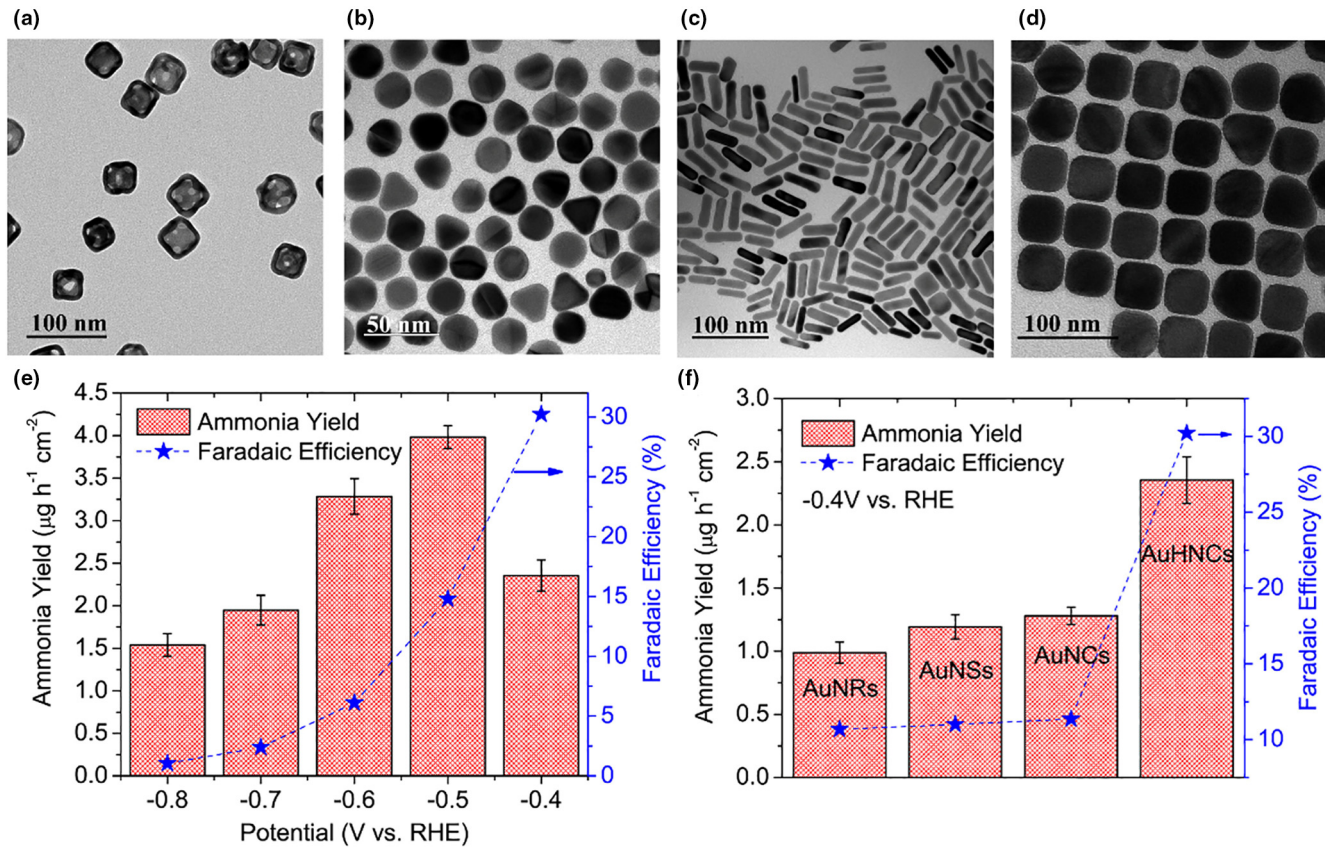
Altering the electronic structures of electrocatalysts is a common strategy for tuning the intrinsic activity of each active site, leading to variations in the atomic arrangement, changes of the adsorption strength of the intermediates and optimization of surface charge-transfer property. In this regard, performing vacancy engineering, heteroatom doping, and strain engineering to realize the modification of electronic configuration of electrocatalysts could be regarded as effective methods to increase the intrinsic activity of the active sites for significantly enhanced electrocatalytic reactivity [30].

Vacancy engineering

The effective strategy to further optimize the catalytic performance in electrocatalysts is introducing various vacancies, such as oxygen [46], sulfur [47], selenium [48], and metal-cation vacancies [49], which could obviously modulate the electronic structure, tune the surface-adsorption property for reaction

intermediates and further enhance the electrocatalytic activities [50]. For example, the existing oxygen vacancies in transition metal oxides could act as the active sites for adsorbing the reactants and reaction intermediates, hence lowering the activation energy barrier, which plays significant role in facilitating the electrochemical reactions [50–53]. Moreover, the introduction of vacancies can favourably affect the electronic structure of catalysts, enabling the enhanced charge transfer and optimal adsorption energetics of intermediates for electrocatalytic reactions [54].

The vacancy engineering can play a very crucial role in the electrocatalytic NRR process. For example, the oxygen vacancies can trap metastable electrons, which may be transferred into an antibonding orbital of adsorbed N₂ molecules, thereby promoting N≡N triple-bond cleavage for subsequent catalytic reaction [55–57]. As reported by Yu's group, Bi₄V₂O₁₁/CeO₂ hybrid with an amorphous phase (BVC-A) containing abundant oxygen vacancies exhibited superior electrocatalytic NRR performance with average ammonia yield of 23.21 µg h⁻¹ mg⁻¹ and corresponding Faradaic efficiency of 10.16% at -0.2 V vs RHE at ambient conditions (Fig. 6c) [57]. It was demonstrated that CeO₂ played a critical role in inducing the amorphous structure of Bi₄V₂O₁₁ and establishing band alignment with Bi₄V₂O₁₁, which could be conductive to electrocatalytic NRR. Remarkably, the disordered structure of amorphous Bi₄V₂O₁₁ were rich in dangling bonds, which can provide high density of defective sites and reduce the energy barrier, serving as a trigger to facilitate the NRR process. Moreover, the established

**FIGURE 5**

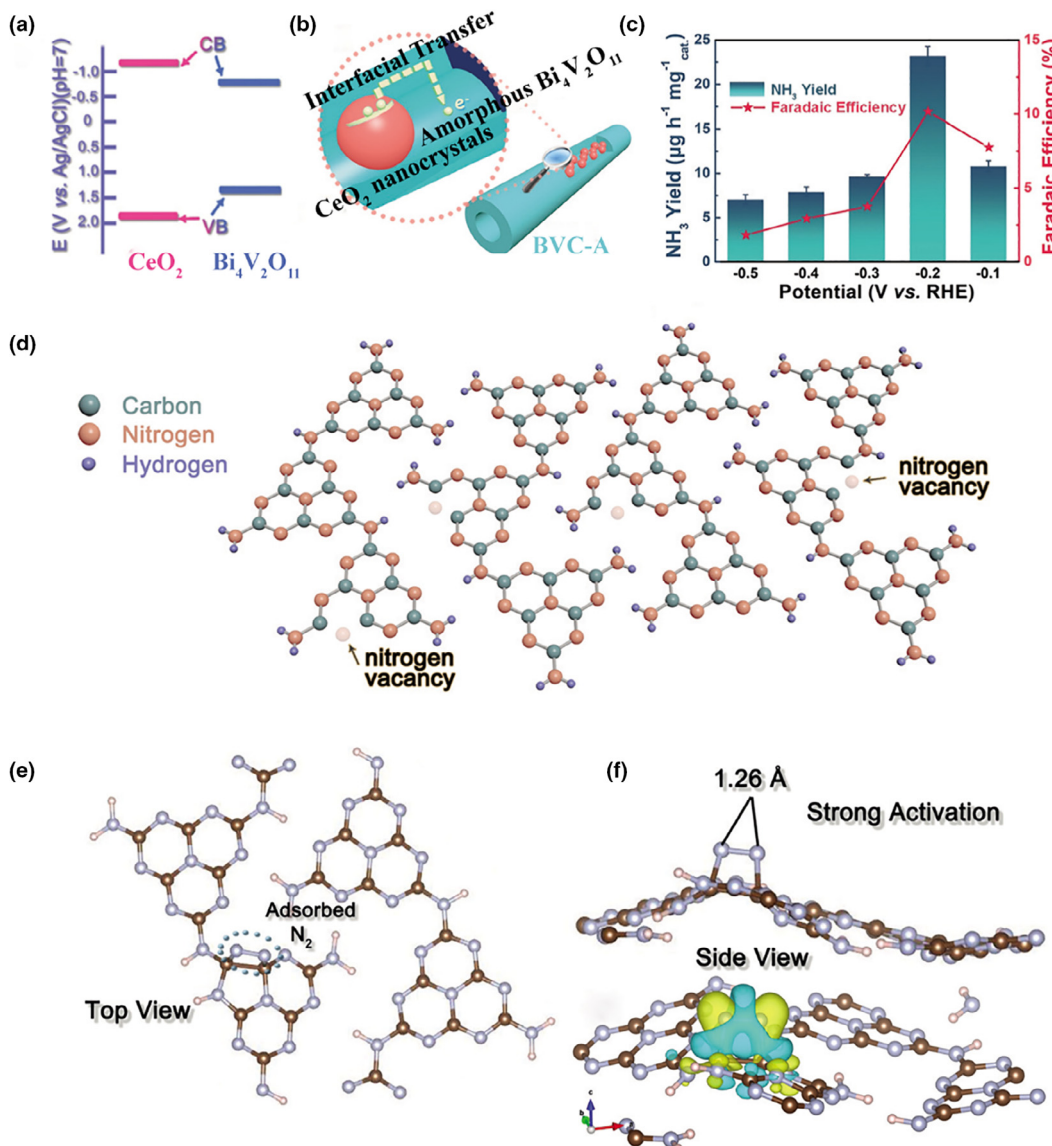
Transmission electron microscope (TEM) images of Au nanoparticles with different shapes for NRR catalysis: (a) Au hollow nanocages (AuHNCs), (b) Au nanospheres (AuNSs), (c) Au nanorods (AuNRs), and (d) Au nanocubes (AuNCs). (e) Ammonia yield and Faradaic efficiency for AuHNCs toward NRR at various potentials. (f) Ammonia yield rate and Faradaic efficiency for Au nanoparticles of various shapes at the potential of -0.4 V vs RHE (reversible hydrogen electrode). Reproduced from Ref. [44] with permission from Elsevier.

band alignment between CeO_2 and $\text{Bi}_4\text{V}_2\text{O}_{11}$ could not only deliver abundant active sites but also facilitate the interfacial charges transfer from CeO_2 to $\text{Bi}_4\text{V}_2\text{O}_{11}$, giving rise to an effective N_2 fixation (Fig. 6a-b). However, the exact role of oxygen vacancies in absorbing N_2 molecules and transforming N_2 to NH_3 was not demonstrated in details neither experimentally nor theoretically. In contrast, the impact of nitrogen vacancies on the electrocatalytic NRR performance are fully confirmed by both theoretical calculations and control experiments in the study of polymeric carbon nitride (PCN) containing a large concentration of tunable nitrogen vacancies (denoted as PCN-NV_x, x represents the heating hours in argon) reported by the same group (Fig. 6d) [58]. Confirmed by theoretical calculations, N_2 molecules could be chemisorbed on nitrogen vacancies of PCN and the bond length of adsorbed N_2 increased significantly leading to the strong N_2 activation (Fig. 6e-f), holding the key to the extraordinary electrocatalytic performance toward NRR. Furthermore, control experiments were conducted with different PCN samples, and it turned out that PCN-NV₄ with abundant nitrogen vacancies achieved the highest NH_3 production rate, manifesting that the boosted NRR activity stemmed from the enrichment of nitrogen vacancies. But, it is worth noting that ¹⁵N₂ isotopic experiments were not carried out, so it is unclarified whether the nitrogen of

NH_3 came from the N_2 applied to the system or the nitrogen-containing electrocatalyst itself.

Heteroatom doping

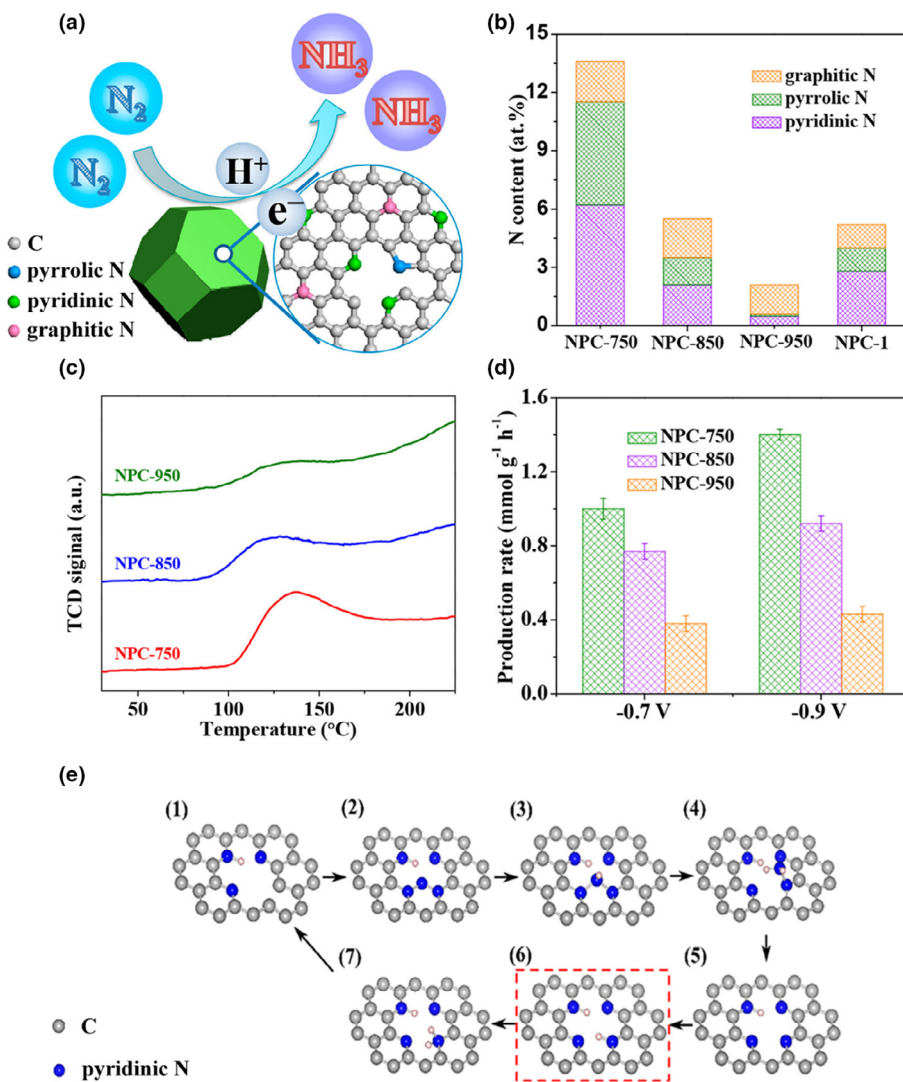
Apart from the vacancy engineering, chemical doping with heteroatoms is another effective strategy for electrocatalytic activity enhancement. The introduction of heteroatoms into the original electrocatalysts could not only modulate the surface electronic structure but also modify the adsorption abilities for reactants or intermediates [59–61]. According to the types of different heteroatoms, it can be roughly divided into two categories, including non-metal-atom doping and metal-atom doping [62]. In the case of non-metal-atom doping, N, S, O, B, and P atoms are usually selected as heteroatoms to modify the electrocatalytic performance of pristine materials. Specifically, the incorporation of non-metal atoms can not only modulate the bandgap of catalysts resulting in enriched charge density and higher intrinsic conductivity but also lower the binding energies of reactants, leading to a low-onset overpotential required to drive the electrocatalytic process [63]. Similar to that of the non-metal-atom doping, doping with foreign metal atoms can also modify the electronic structures and optimize the absorption free energy toward intermediates for improved electrocatalytic activity [64,65].

**FIGURE 6**

(a) Band alignment of Bi₄V₂O₁₁/CeO₂ hybrid with an amorphous phase (BVC-A). (b) Illustration of interfacial charge transfer in BVC-A. (c) NH₃ yield and Faradaic efficiency of BVC-A toward NRR at different potentials. Reproduced from Ref. [57] with permission from Wiley-VCH. (d) Schematic illustration of nitrogen vacancies on polymeric carbon nitride (PCN). (e) N₂ adsorption geometry on PCN with nitrogen vacancy. (f) The charge density difference of the N₂-adsorbed PCN with nitrogen vacancy; the yellow and blue isosurfaces represent charge accumulation and depletion in the space, respectively. Reproduced from Ref. [58] with permission from Wiley-VCH.

In the field of electrocatalytic NRR, the application of heteroatom doping mainly focused on carbon-based materials. Nitrogen is an effective heteroatom for tuning the NRR activity of carbon-based materials primarily because nitrogen doping can alter the electronic structures of the nearby carbon atoms and create defects to enable stronger adsorption of reactant molecules [62]. The nitrogen-doping content and doping sites may be the decisive factors in nitrogen adsorption and ammonia synthesis, yet there is a disagreement regarding which types of nitrogen-doping contribute to the N₂ reduction to NH₃. In a previous study by Liu and coworkers, N-doped porous carbon (NPC) was reported as a cost-effective NRR electrocatalyst (Fig. 7a), where the correlation between the level of N doping and NRR performance was revealed by the experiments combined with DFT cal-

culations [66]. The electrochemical N₂ reduction tests were carried out between NPC samples synthesized under different carbonization temperatures of 750, 850, or 950 °C (denoted as NPC-750, NPC-850, and NPC-950) containing various doped N contents and species (Fig. 7b). The experimental results indicated that the ammonia production activity could be enhanced with increased N-doping content (especially pyridinic N) due to more stronger N₂ adsorption on NPC confirmed by temperature-programmed desorption of N₂ (N₂-TPD) (Fig. 7c-d). DFT calculations further revealed that pyridinic and pyrrolic N were active sites for ammonia production and their contents were crucial for promoting ammonia synthesis on NPC. However, ¹⁵N₂ isotopic experiments are required to prove that the nitrogen source of detected ammonia generated from N₂ reduction rather than

**FIGURE 7**

(a) Schematic illustration of NRR process of N-doped porous carbon (NPC). (b) Contents of pyridinic, pyrrolic, and graphitic nitrogen in NPCs synthesized at different temperatures. (c) N_2 temperature-programmed desorption (N_2 -TPD) of NPCs. (d) Ammonia production rates of NPCs at -0.7 and -0.9 V. Reproduced from Ref. [66] with permission from American Chemical Society. (e) Atomistic structure scheme showing the reaction pathway of the N_2 reduction in the N_3 sites. Reproduced from Ref. [67] with permission from Elsevier.

nitrogen atoms of NPC. Similarly, Mukherjee et al. investigated the NRR performance of nitrogen-doped nanoporous carbon derived from metal-organic framework. They studied the effects of nitrogen-doping content and doping site on ammonia yield rates of the disordered carbon catalysts synthesized at different carbonization conditions, including heating temperature and duration [67]. It was demonstrated that the catalysts prepared at conditions of $1100\text{ }^{\circ}\text{C}$ and 1 h with dominant pyridinic and graphitic N doping exhibited a remarkable NH_3 production rate of $3.4 \times 10^{-6}\text{ mol cm}^{-2}\text{ h}^{-1}$ with a Faradaic efficiency (FE) of 10.2% at a relatively low overpotential. DFT calculations further elucidated that the carbon moiety consisting of three pyridinic N atoms (N_3) and one adjacent carbon vacancy acted as active sites, which could provide strong adsorption of N_2 molecules and realize the cleavage of $N\equiv N$ triple bond for subsequent N_2 protonation process (Fig. 7e). Still, the nitrogen atoms doped in the carbon materials might participate in the ammonia production

process, which could influence the ammonia determination results.

Strain engineering

In recent years, it is of growing importance to optimize the electrocatalytic activity of nanomaterials by tuning or controlling the surface strain of the electrocatalysts, which can tailor the surface electronic structure via altering the surface atomic spacing and the atomic bond length [61,68–70]. The utilization of shape or volume controllable substrate to introduce strain into deposited metal catalysts has been regarded as an effective strategy for tuning the catalytic activity of electrocatalysts [68]. Cui's group applied volume tunable lithium (Li)-ion battery electrode materials ($LiCoO_2$) as catalyst support to control the lattice strain of deposited Pt catalysts, thus tuning its catalytic activity for the ORR [71]. The intercalation and extraction of Li ions during electrochemical charge and discharge process could change the

volume and lattice spacing of layered LiCoO₂, therefore inducing either compressive or tensile strain in Pt catalysts. As a result, Pt catalysts exhibited 90% enhancement or 40% suppression in ORR activity under compression or tension, respectively. The strain engineering strategy can be further extended by integrating crystal strain with defects, including heteroatoms and lattice vacancies, to improve the electrocatalytic performance. Qiao's group reported that cobalt(II) oxide nanorods could be turned into efficient electrocatalysts for HER with the aid of surface strain engineering coupled with the creation of abundant oxygen vacancies [72]. It was demonstrated that the tensile strain can strongly modulate the atomic, electronic structures, and the surface reactivity of CoO nanorods, while the oxygen vacancies facilitate water dissociation and lower the hydrogen adsorption free energy, contributing to an enhanced electrocatalytic activity toward HER. Moreover, the synergistic effect of the crystal strain and the phase transformation is beneficial to the modulation of electrocatalytic performance, especially for transition-metal chalcogenides. For instance, Voiry et al. investigated the influence of strain induced by zigzag-like local lattice distortions and phase transformation on the catalytic activity of chemically exfoliated WS₂ nanosheets [70]. Experimental results indicated that the exchange current density gradually decreased with lower 1T (octahedral) fraction and reduced strain, suggesting that the catalytic activity for HER are strongly linked to both the 1T phase concentration and the strain. The DFT calculations further revealed that the 1T WS₂ phase is more catalytically active compared with 2H (trigonal prismatic) phase, and the strain could significantly lower the atomic hydrogen adsorption free energy of distorted 1T WS₂, therefore, enhancing the electrocatalytic activity toward HER. To date, although having not been put into practice, the application of strain engineering strategy in electrocatalytic N₂ reduction to NH₃ might open a new avenue for the development of high-performance NRR catalysts.

Efficient NRR electrocatalysts

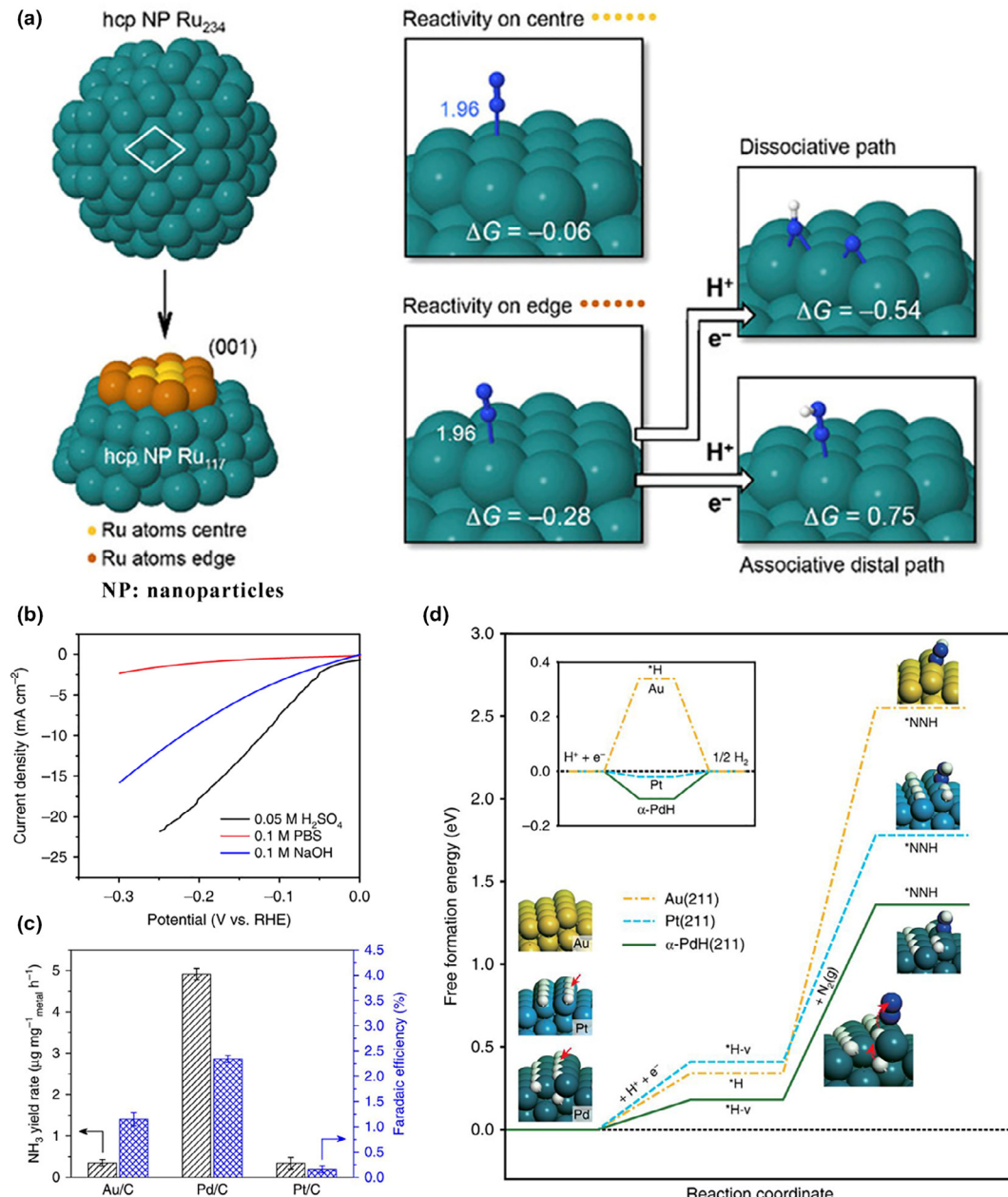
Development of efficient electrocatalysts is essential for supporting an optimized conversion process of nitrogen to ammonia. In recent years, various electrocatalysts catalyzing the NRR at ambient conditions have been explored, including noble metal-based materials, non-noble metal-based materials, single-metal-atom catalysts, and metal-free materials. In this section, the investigation of the electrocatalytic NRR performance of these materials correlated with material design strategies and inherent properties of selected catalysts will be discussed in detail.

Noble metal-based materials

Noble metal materials have been demonstrated as promising electrocatalysts for a wide range of electrochemical reactions (e.g., HER, OER, and ORR) in virtue of their superior electrical conductivity, high-density of under-coordinated surface atoms and appropriate adsorption of various reactants [73,74]. Recently, noble metals have been widely applied as excellent electrocatalysts for ammonia synthesis under ambient conditions. For example, Ru nanoparticles grown on a carbon fiber paper as NRR electrocatalysts were reported to achieve high Faradaic efficiency of 5.4% at 10 mV vs RHE [75]. It is worth noting

that the ability to enable NRR at potentials close to RHE could improve the Faradaic efficiency for NRR and render the H₂ viable as byproduct. Evidenced by the DFT calculations, the low overpotential for catalyzing NRR is ascribed to the instantaneous N₂ adsorption on the catalytic edge sites of hcp Ru (0 0 1) nanoparticles and the spontaneous hydrogenation of the adsorbed N₂ leading to the cleavage of the N≡N bond followed by an electrochemically promoted dissociative pathway (Fig. 8a), demonstrating excellent catalytic ability of Ru nanoparticles. In addition, the formation of noble metal hydride could accelerate N₂ hydrogenation, thus enhancing NH₃ production rate. Wang et al. investigated the electrocatalytic reduction of N₂ to NH₃ on carbon black-supported palladium nanoparticles (Pd/C), which exhibited an NH₃ yield rate of ~ 4.5 μg h⁻¹ mg⁻¹ and a Faradaic efficiency of 8.2% at 0.1 V vs RHE when operating in phosphate buffer solution (PBS) electrolyte [22]. To demonstrate the effective suppression of the HER in PBS electrolyte, the HER activities of the Pd catalysts in different electrolytes, including 0.05 M H₂SO₄, 0.10 M PBS, and 0.10 M NaOH, were compared, and the corresponding linear sweep voltammetric (LSV) curves along with electrochemical impedance spectra (EIS) revealed the less favorable kinetics of HER in PBS due to a higher barrier for the mass diffusion and charge transfer (Fig. 8b). In addition, control experiments suggested that Pd was more active for NRR compared with Au and Pt nanoparticles with similar sizes (Fig. 8c), because Pd could absorb H atoms in its lattice and form α-PdH that lowered the free energy barrier of N₂ hydrogenation as evidenced by the DFT calculations (Fig. 8d).

The electrochemical characteristics of noble metals can be elaborately modulated by controlling their geometric structures and electronic states, consequently their catalytic performance toward NRR process can be finely tuned [31]. Specifically, the controllable synthesis of noble metal with different morphologies is crucial to investigate the structure–property relationship and modify the NRR performance by tuning the geometric structure. For instance, flower-like Au microstructure assembled by staggered nanoplates as building blocks was synthesized as an electrocatalyst for the NRR [76]. As-prepared flower-like Au catalysts exhibit a high FE of 6.05% and ammonia production rate of 25.57 μg h⁻¹ mg⁻¹ at -0.2 V vs RHE under ambient conditions, which outperform the Au sphere counterpart due to larger electrochemically active surface areas. The excellent catalytic NRR performance of Au flowers was highly correlated to the highly dendritic structures, which provide abundant electrocatalytically active sites for the NRR. However, capping agent (e.g., polyvinyl pyrrolidone (PVP)) used in the synthesis process might remained on the noble metal surface and block the active sites, exerting detrimental influence on surface catalytic reaction [77]. Therefore, morphology-controlled synthesis in the absence of capping agents would be beneficial for achieving desired catalytic properties of noble metals. For example, surfactant-free ultrathin Rh nanosheets with clean surface were successfully synthesized and used for electrochemical reduction of N₂ to NH₃ [78]. The Rh nanosheets showed a high NH₃ yield of 23.88 μg h⁻¹ mg⁻¹ at -0.2 V vs RHE, benefiting from the high specific surface area, the modified electronic structure, and abundant low-coordinate defective atoms on the catalyst surface. But, the Faradaic efficiency at the same potential was only 0.217% far below the level

**FIGURE 8**

(a) Density functional theory (DFT) calculation models for Ru NP (nanoparticles). Reproduced from Ref. [75] with permission from Wiley-VCH. (b) Linear sweep voltammetric curves of the Pd/C catalyst measured in different electrolytes. (c) Comparison of the Pd/C with Au/C and Pt/C for electrocatalytic NRR. (d) DFT-calculated free energy pathways of HER (inset) and the relevant steps of NRR on the (211) surfaces of Au, Pt, and α -PdH at surface potential of 0 V vs RHE (reversible hydrogen electrode) under 298.15 K (atomic structures shown in the insets). Reproduced from Ref. [22] with permission from the Nature Publishing Group.

of other noble metal catalysts, which was attributed to the dominant HER process occupying most of the active sites.

Even though noble metals exhibit superior electrocatalytic activity toward NRR, their large-scale applications are severely impeded by the high costs and rare resources. To overcome these obstacles, the combination of noble metals and carbon materials as composites may represent a new route for reducing the usage of noble metals, as well as optimizing the catalytic performance. For example, Wang et al. reported that the construction of composites consisting of nitrogen-doped nanoporous graphitic

carbon membrane (NCM) and Au nanoparticles could dramatically enhance the FE and NH₃ yield rate to 22% and 0.36 g m⁻² h⁻¹, respectively [79]. The NCM, as the loading support, owned three-dimensional (3D) interconnected macroporous architecture to accelerate the mass diffusion and charge transfer, and the introduced N heteroatoms served to modify the electronic structure of the graphitic carbons for improving catalytic performance. Besides, the synergistic charge transfer between the NCM and Au could promote the N₂ adsorption and thereby enhance the conversion of N₂ to NH₃. To further promote the catalytic

activity of noble metal-based composites, the amorphization strategy could be applied to induce more defects acting as active sites. For example, Yan's group utilized CeO_x to transfer crystallized Au into amorphous phase and introduced reduced graphite oxide (RGO) as substrate to anchor the Au nanoparticles while maintaining good dispersion [80]. As a result, the obtained amorphous Au/ CeO_x -RGO with low Au loading (1.31 wt%) endowed excellent NRR performance with high Faradaic efficiency of 10.10 % and ammonia production rate of $8.3 \mu\text{g h}^{-1} \text{mg}^{-1}$ at -0.2 V vs RHE , which are significantly higher than those of the crystalline Au/RGO. Compared with the crystalline counterpart, the amorphous composite possessed numbers of unsaturated coordination sites with a stronger binding ability of N_2 molecules and improved chemical reactivity for converting N_2 into NH_3 . Moreover, alloying strategy could also be utilized to create multiple reactive sites and modify the electronic structures, as demonstrated by Yan's group in the study of Pd-Cu bimetallic alloys anchored on RGO ($\text{Pd}_{0.2}\text{Cu}_{0.8}/\text{RGO}$) [81]. By adjusting the stoichiometric ratio of Pd and Cu, the optimized NRR performance can be achieved for $\text{Pd}_{0.2}\text{Cu}_{0.8}/\text{RGO}$ composite with NH_3 yield rate of $2.80 \mu\text{g h}^{-1} \text{mg}^{-1}$ at -0.2 V vs RHE . The superior catalytic activity of bimetallic composite can be attributed to the alloying effect and the exposure of more active sites enabled by RGO support.

Non-noble metal-based materials

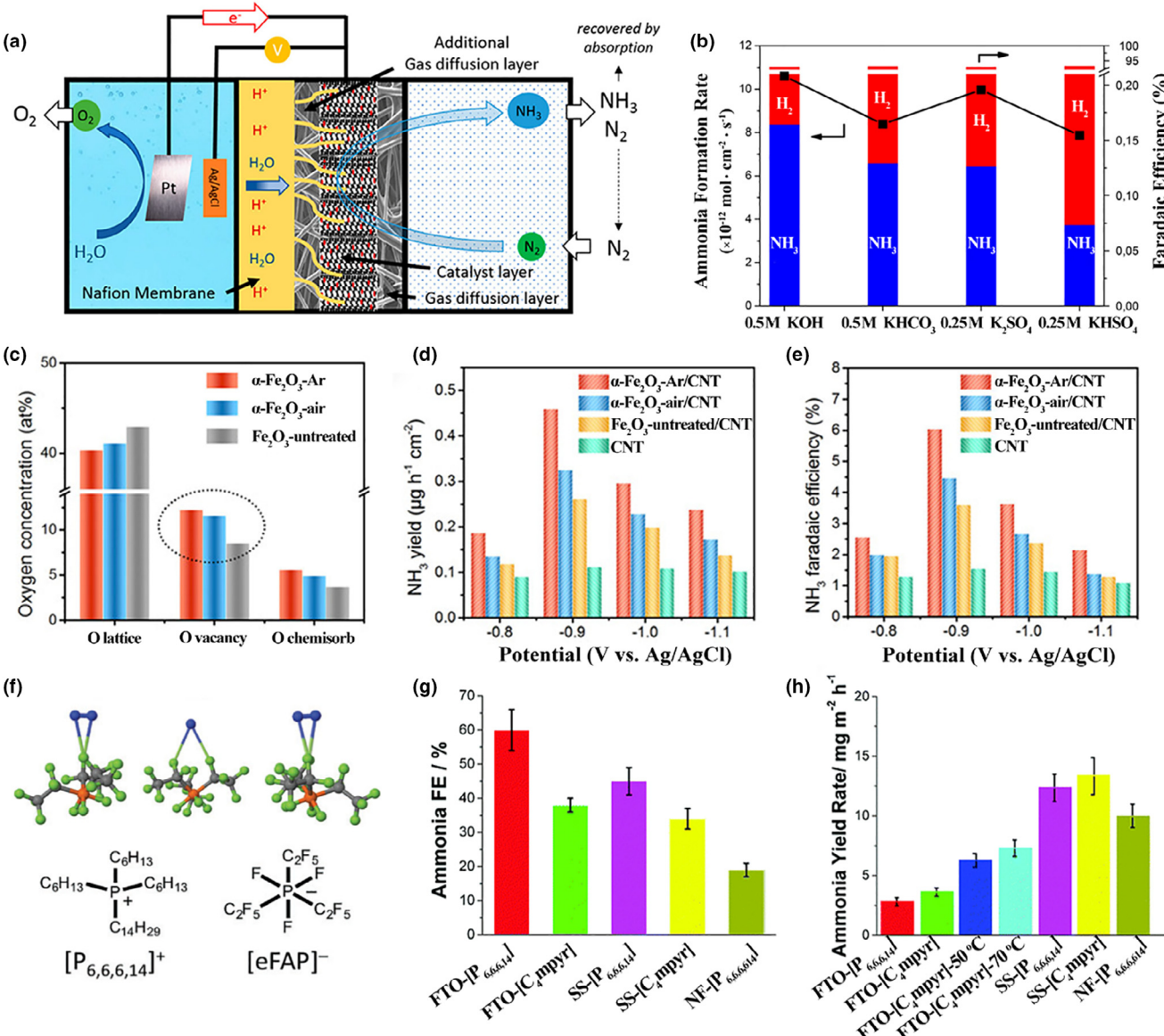
Recently, non-noble metals (especially transition metals) have been regarded as alternative NRR electrocatalysts of noble metals owing to their low cost, abundant resources, and desirable catalytic activity. Up to now, transition metal-based materials, including oxides, chalcogenides, nitrides, carbides, phosphides, and their composites, have been reported as efficient electrocatalysts toward the NRR under ambient conditions. Owning to the limited investigations on transition metal chalcogenides [82,83] and phosphides [84], the NRR performance of which might deserve further validation, emphasis would be placed on oxide-, nitride-, and carbide-based catalysts in this section.

Transition metal oxide-based materials

In terms of transition metal oxides, despite various oxides, including Cr_2O_3 , MoO_3 , and Nb_2O_5 , have been reported [85–87], most investigations mainly focused on Fe-based oxides catalysts. Ever since electrochemical ammonia synthesis by nano- Fe_2O_3 was reported by Licht et al. [6], Fe-based materials have drawn wide attention as efficient NRR electrocatalysts under mild conditions. Considering hematite ($\alpha\text{-Fe}_2\text{O}_3$) is the most thermodynamically stable form of iron oxides, DFT calculations were utilized to investigate the electrochemical formation of NH_3 molecules on hematite (0001) surfaces terminated by single-iron ($\text{Fe}-\text{O}_3-\text{Fe}-$) or double-iron ($\text{Fe}-\text{Fe}-\text{O}_3-$) [88]. It turned out that N_2 reduction mechanism followed the associative pathway and the applied bias for proton transfer in the $\text{Fe}-\text{Fe}-\text{O}_3-$ surface was smaller due to the two available reactive Fe sites on this surface, which confirmed the catalytic activity of Fe sites in iron oxides theoretically. Chen et al. investigated the NRR performance of iron oxide supported on carbon nanotubes (Fe_2O_3 -CNT) at room temperature and atmospheric pressure [89]. A maximum NH_3 formation rate of $0.22 \mu\text{g h}^{-1} \text{cm}^{-2}$ was obtained under an

applied potential of -2.0 V ; however, the corresponding Faradaic efficiency was quite low (<0.15%) due to the side reaction of hydrogen evolution. The experiment data indicated that the active sites generated at the interface between iron particles and CNT might be able to activate N_2 and make it more reactive toward hydrogenation. Furthermore, the same group dedicated to optimize both Fe_2O_3 /CNT electrocatalyst and reactor/reaction conditions to enhance the efficiency of the NRR process [90]. To improve cell design, an additional gas diffusion layer was inserted in between the electrocatalyst layer and the Nafion membrane for avoiding the crossover of ammonia through the Nafion membrane into the anode chamber (Fig. 9a). Based on the investigation of the effects of iron content and electrolyte (composition, pH, and concentration) on the catalytic activity of Fe_2O_3 /CNT, an ammonia yield rate of $1.06 \times 10^{-11} \text{ mol cm}^{-2} \text{ s}^{-1}$ with Faradaic efficiency of 0.164% was obtained for the 30% Fe_2O_3 /CNT electrocatalyst in 0.5 M KOH electrolyte (Fig. 9b). By altering the applied voltage, the best ammonia formation rate was observed at $-2.0 \text{ V vs Ag/AgCl}$, but suffering from poor stability caused by the reduction in iron oxides. In order to further improve the NRR performance of Fe-based nanostructured catalysts, Zhang's group introduced more oxygen vacancies to the hematite surface and explored the effects of oxygen vacancies concentration on electrocatalytic activity of $\alpha\text{-Fe}_2\text{O}_3$ prepared at different oxygen partial pressure during annealing process (Fig. 9c) [91]. At an applied voltage of $-0.9 \text{ V vs Ag/AgCl}$, a highest NH_3 formation rate ($0.46 \mu\text{g h}^{-1} \text{cm}^{-2}$) and a maximum FE (6.0%) can be obtained by the $\alpha\text{-Fe}_2\text{O}_3$ -Ar/CNT catalyst with abundant oxygen vacancies resulting from annealing process in argon (Fig. 9d–e). The experiment results demonstrated that the hematite surface structure modification with more oxygen vacancies could facilitate adsorption and activation of N_2 molecules and accommodate more active sites to boost the conversion of N_2 to NH_3 through pathways with low energy barriers. However, the NRR performance would degrade over longer duration due to the reduction in $\alpha\text{-Fe}_2\text{O}_3$ and the degradation of the Nafion membrane [91].

In addition to Fe_2O_3 , Fe-based materials in other chemical states (such as Fe and Fe_3O_4) can also be catalytically active for NRR. Hu et al. investigated the influence of chemical state and composition of Fe-based catalysts on their NRR activity and selectivity [92]. It was found that the obtained $\text{Fe}/\text{Fe}_3\text{O}_4$ catalyst exhibited improved activity and selectivity toward NRR in comparison to commercial Fe, Fe_3O_4 , and $\alpha\text{-Fe}_2\text{O}_3$ nanoparticles, achieving a FE of 8.29% for NH_3 synthesis at -0.3 V vs RHE . Apart from the design of Fe-based catalysts, the optimization of electrolyte aiming at limiting the availability of protons could effectively suppress the competing HER and thus improving NRR selectivity [93]. For this purpose, MacFarlane's group selected ionic liquids ($[\text{C}_4\text{mpyr}][\text{eFAP}]$ or $[\text{P}_{6,6,6,14}][\text{eFAP}]$) (Fig. 9f) mixed with trace amounts of water as electrolyte to electrochemically synthesize NH_3 from N_2 over a nanostructured iron catalyst [94]. A higher NH_3 yield rate was obtained in $[\text{C}_4\text{mpyr}][\text{eFAP}]$ ionic liquids compared with $[\text{P}_{6,6,6,14}][\text{eFAP}]$, consistent with the difference of viscosity, whereas the highest FE (60%) was achieved in $[\text{P}_{6,6,6,14}][\text{eFAP}]$ due to the high solubility of N_2 (Fig. 9g–h). The DFT calculations further revealed that the strong delocalization of negative charge in the $[\text{eFAP}]^-$ could

**FIGURE 9**

(a) Schematic view of the improved cell design for electrochemical ammonia synthesis over $\text{Fe}_2\text{O}_3/\text{CNT}$. (b) Ammonia formation rate and Faradaic efficiency of 30% $\text{Fe}_2\text{O}_3/\text{CNT}$ in different electrolyte. Reproduced from Ref. [90] with permission from American Chemical Society. (c) Comparison of the concentration of three different oxygen species of $\alpha\text{-Fe}_2\text{O}_3\text{-Ar}$, $\alpha\text{-Fe}_2\text{O}_3\text{-air}$, and $\text{Fe}_2\text{O}_3\text{-untreated}$ (annealed in different atmosphere). (d) NH_3 yield rate and (e) Faradaic efficiency of different catalysts at different applied potentials. Reproduced from Ref. [91] with permission from Wiley-VCH. (f) Structures of the ionic liquid ions and their interaction with N_2 . (g) FE and (h) NH_3 yield rate of iron catalyst deposited on various electrodes (fluorine doped tin oxide glass (FTO), nickel foam (NF), and stainless steel cloth (SS)) when using different ionic liquids at -0.8 V vs NHE (normal hydrogen electrode). Reproduced from Ref. [94] with permission from the Royal Society of Chemistry.

enhance the strength of N_2 binding, thus resulting in the high N_2 solubility. Although superior NRR selectivity was achieved in $[\text{P}_{6,6,6,14}][\text{eFAP}]$ as a result of limitation of proton supply and high N_2 solubility, the corresponding NH_3 yield rate ($2.9 \text{ mg m}^{-2} \text{ h}^{-1}$) was relatively low because the N_2 mass transport was hindered in the viscous ionic liquids [94].

Transition metal nitride-based materials

Under the circumstance of comprehensive DFT investigations on a range of transition metal nitrides (TMN) for catalyzing electrochemical nitrogen reduction to produce ammonia, metal nitrides are believed more active toward NRR than toward HER compared

with pure metal catalysts [95–98]. Abghouei et al. proposed that nitrogen electroreduction to ammonia on the TMN surface followed a favorable Mars-van Krevelen (MvK) mechanism, in which a surface N atom of TMN can in principle be reduced to NH_3 , and the created N vacancy is then replenished by N_2 molecule to endure the catalytic cycle [98]. Based on the MvK mechanism, a series of DFT calculations were carried out to compare the catalytic activity and stability of various TMN when considering the possibility of N vacancy poisoning and the likelihood of catalyst decomposition and regeneration [97]. The most promising nitride candidates were found to be ZrN, NbN, CrN, and VN with the (100) facets of rocksalt structure, which were

expected to catalyze electrochemical ammonia synthesis at smaller overpotentials of around -0.5 to -0.8 V [96]. Although a range of metal nitrides were proven to be promising NRR catalysts through theoretical analyses, only Mo- and V-based nitrides have been experimentally proven to show good catalytic activity toward NRR [99–103], in which the identification of nitrogen source of produced ammonia and the validation of reaction mechanism are extremely vital. Yang and coworkers conducted investigations on the NRR performance of vanadium nitride (VN) nanoparticles and combined ex situ and operando characterizations to provide mechanistic insights into the reaction process [103]. An ammonia production rate of $3.3 \times 10^{-10} \text{ mol s}^{-1} \text{ cm}^{-2}$ was obtained on the VN catalyst at -0.1 V within the first hour but with a decrease of 62% during longer duration (5–8 h), while nearly no ammonia could be detected after 1 h on VN catalyst at applied potentials below -0.2 V (Fig. 10a). X-ray photoelectron spectroscopy (XPS) along with Operando X-ray absorption spectroscopic (XAS) revealed that the surface $\text{VN}_{0.7}\text{O}_{0.45}$ species as the active phase for NRR would be converted to VN during the nitrogen reduction process, causing the reduced ammonia yield rate during long time reaction. In addition, the $\text{VN}_{0.7}\text{O}_{0.45}/\text{VN}$ ratio after NRR decreased with more negative potentials until -0.2 V meaning large fraction of exposed $\text{VN}_{0.7}\text{O}_{0.45}$ was converted, which might explain the rapid deactivation of catalyst at applied potential of -0.2 V. Furthermore, $^{15}\text{N}_2$ isotopic experiments showed that both $^{14}\text{NH}_3$ and $^{15}\text{NH}_3$ were detected with the feed of $^{15}\text{N}_2$ indicating that the reaction process followed the MvK mechanism. On the basis of the DFT calculations, reactivity experiments, and characterization results, it was hypothesized that only the surface N atoms adjacent to a surface O serve as active sites for catalyzing NRR and more negative potentials would lead to the replacement of unstable surface O atoms by N atoms from N_2 feed, resulting in the formation of inactive VN phase accompanied by the deactivation of catalyst (Fig. 10b).

Transition metal carbide-based materials

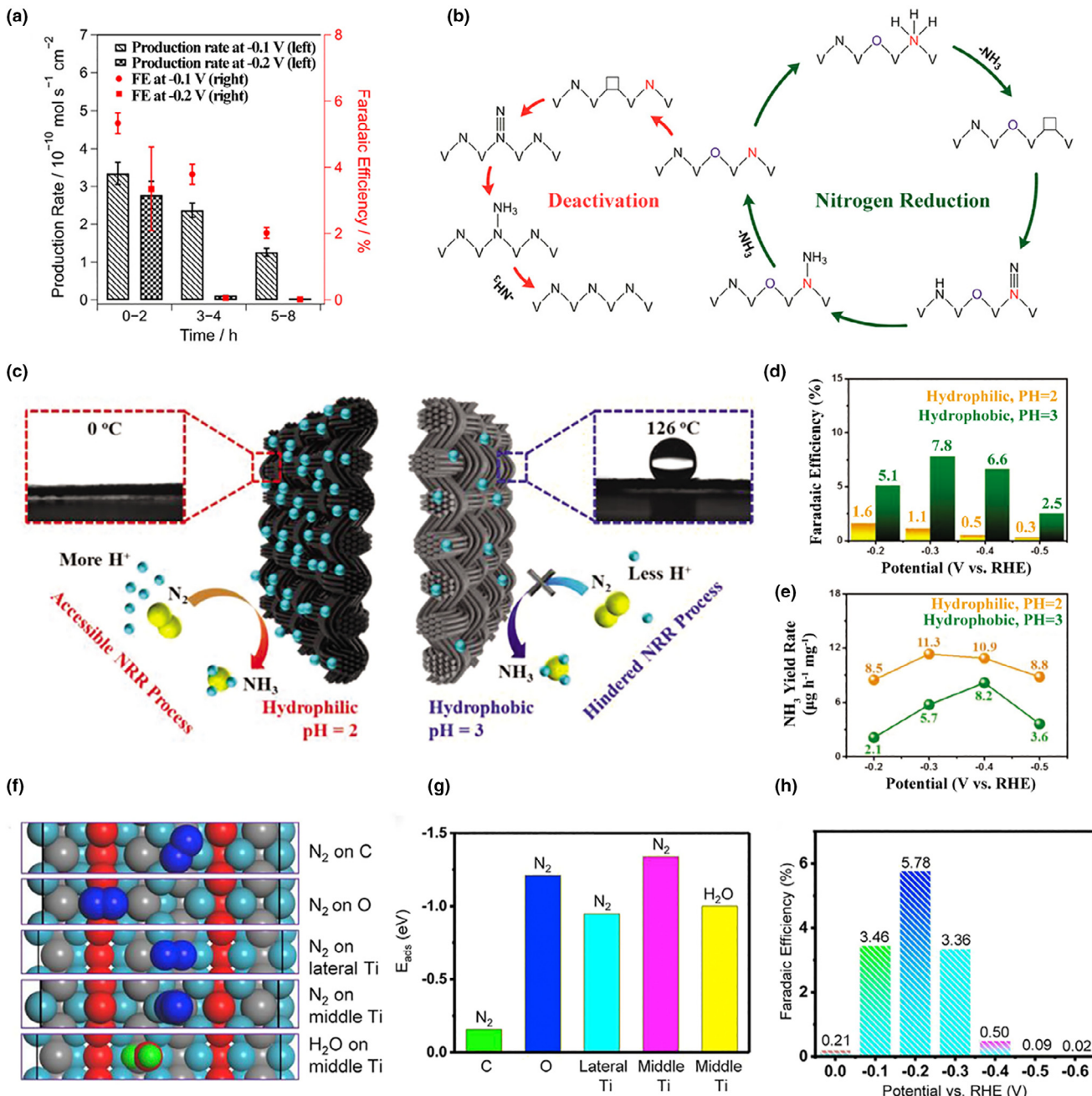
In terms of transition metal carbides, DFT investigations suggested that MXenes (two-dimensional layers of transition metal carbides) from the d^2 , d^3 , and d^4 series with the general formula M_3C_2 were promising catalysts for N_2 capture and reduction [104]. The spontaneous N_2 chemisorption on MXene nanosheets could induce the elongation of the $\text{N}\equiv\text{N}$ triple bond, promoting the catalytic conversion of N_2 into NH_3 . Due to the reduced activation barrier, low overpotentials of 0.64 V and 0.90 V vs SHE (standard hydrogen electrode) could be obtained in the case of V_3C_2 and Nb_3C_2 , respectively. Another computational study conducted by Matanovic et al. investigated the viability of cubic molybdenum carbide (MoC) as a NRR electrocatalyst [105]. The comparison between the N atoms and H atoms adsorption energies of various crystallographic surfaces of cubic MoC revealed that the nitrogen reduction in MoC (1 1 1) surface could proceed at small negative potentials of -0.3 V vs. SHE due to the stronger N atoms adsorption. Besides, the hydrogen evolution could be suppressed via introducing carbon vacancies to prevent the accumulation of H-adatoms. The NRR catalytic activity of transition metal carbides was further confirmed by Wang's group via developing molybdenum carbide nanodots embedded in ultrathin

carbon nanosheets ($\text{Mo}_2\text{C}/\text{C}$) as a highly efficient catalyst for electrochemical N_2 fixation [20]. The obtained $\text{Mo}_2\text{C}/\text{C}$ nanosheets exhibited excellent NRR catalytic performance with a high NH_3 production rate of $11.3 \mu\text{g h}^{-1} \text{ mg}^{-1}$ due to the abundant active sites of Mo_2C nanodots for favorable N_2 adsorption and unique electronic structure beneficial for the activation of $\text{N}\equiv\text{N}$ bond and catalytic hydrogenation. Importantly, the influence of hydrogen evolution on the catalytic activity of $\text{Mo}_2\text{C}/\text{C}$ nanosheets toward NRR was investigated by controlling the availability of protons (Fig. 10c). The NRR performance control experiments between proton-enriched condition and proton-suppressed condition revealed that the suppressed proton supply could significantly enhance the Faradaic efficiency but at the expense of decreased NH_3 yield rate, indicating that excessive suppression of hydrogen evolution might deteriorate the NRR performance of catalysts (Fig. 10d–e). Under this circumstance, the $\text{Mo}_2\text{C}/\text{C}$ nanosheets were capable of catalyzing NRR process under ambient conditions even though accompanied with hydrogen evolution. Also, the same group explored the possibility of using 2D MXene (e.g., $\text{Ti}_3\text{C}_2\text{T}_x$ nanosheets) attached to a vertically aligned metal host (e.g., FeOOH nanosheets) for the conversion of N_2 into NH_3 by tuning the exposed active sites and inhibiting hydrogen evolution [106]. Based on the DFT calculations of the N_2 adsorption energy on various active sites of MXene, the middle Ti atoms on the edge plane turned out to be the most active sites for preferential N_2 adsorption compared to the sites on the basal plane with an unfavorable energy barrier (Fig. 10f–g). To confirm the DFT results, the NRR activity comparison of MXenes with different sheet sizes was carried out and it revealed that the small MXene sheets showed better NRR performance than the large sheets due to the exposure of more active edge sites. Furthermore, compared with other metal hosts, the vertically aligned FeOOH nanosheets as the support of MXene sheets could enhance the Faradaic efficiency to 5.78% at -0.2 V vs RHE (Fig. 10h), which was ascribed to the increased number of exposed active edge sites and the sluggish kinetics of FeOOH toward HER.

Single-metal-atom catalysts

Single-atom catalysts containing isolated metal atoms dispersed on support materials have emerged as promising electrocatalysts due to the homogenized catalytically active centers, the uniform low-coordination environment and maximal active metal atoms utilization, endowing them with enhanced catalytic activity, stability, and selectivity for various electrochemical applications [107,108]. To date, single-transition metal atoms anchored on different supporting substrates (such as carbon materials [109], boron nitride [110], phosphorene [111], and molybdenum disulfide [112]) have been proven efficient toward electrochemical nitrogen-to-ammonia conversions by theoretical calculations, whereas the catalytic activity of single-atom catalysts need further validation through experiments.

To achieve highly active single-atom catalysts, the deliberate selection of appropriate supporting substrates are of vital importance for stabilizing the metal atoms dispersed on the support and establishing strong metal-support interactions [108]. Specifically, N-doped carbon materials have been regarded as promising supporting substrates for anchoring metal atoms by the

**FIGURE 10**

(a) Production rate and Faradaic efficiency of VN catalysts for 8 h tests at -0.1 V and -0.2 V, respectively. (b) Proposed reaction pathway for nitrogen reduction and catalyst deactivation on the surface of $\text{VN}_{0.7}\text{O}_{0.45}$. Reproduced from Ref. [103] with permission from American Chemical Society. (c) NRR catalytic mechanism of the $\text{Mo}_2\text{C}/\text{C}$ under proton-suppressed and proton-enriched conditions. (d) Faradaic efficiency and (e) NH_3 yield rate of the $\text{Mo}_2\text{C}/\text{C}$ at different potentials under proton-suppressed and proton-enriched conditions. Reproduced from Ref. [20] with permission from WILEY-VCH. (f) Optimized structures and (g) the corresponding adsorption energy (E_{ads}) values for N_2 on various atomic sites of MXene. (h) Faradaic efficiency of MXene/FeOOH at various potentials. Reproduced from Ref. [106] with permission from Elsevier.

formation of atomic metal–nitrogen–carbon moieties (M–N–C), contributing to a good atomic stability and high catalytic activity. For instance, the NRR catalytic performance of a series of single-metal atoms anchored on N-doped carbon was investigated by employing first-principle calculations [113]. It turned out that $\text{Mo-N}_1\text{C}_2$ (the single-Mo atom coordinated by a N atom and two C atoms) served as the active sites for catalyzing NRR due to the strong N_2 -binding ability (N_2 adsorption energies of -1.19 eV),

ultralow overpotential of only 0.24 V, and rapid removal of synthesized NH_3 (NH_3 desorption energies of 0.47 eV). Apart from the dramatic improvement of NRR catalytic activity, a significant suppression of HER can also be achieved for single-atom catalysts supported on defective graphene derivatives as demonstrated by Choi et al [114]. In particular, the effect of adsorption site and electronic structure on H adsorption and N_2 binding ability was investigated by DFT calculations. The comparison of H

adsorption free energy on different adsorption sites indicated that the adsorbed H was unstable on the top site, the only available adsorption site on single-atom catalysts, meaning the hindered H adsorption and thus the suppressed HER. In addition, the interactions between metal atoms and support could effectively modify electronic structure of single-atom catalysts and transfer some positive charge to the active metal sites, leading to the easier polarization of metal d-orbitals and the favorable N₂ binding. Besides, on the basis of calculation of formation energies, single-atom Ti and V catalysts can be easily synthesized in nitrogen-rich conditions owing to the relatively low formation energies. In addition to carbon materials, the boron nitride (BN) nanosheet with abundant point defects can also be utilized to support the single-metal atom for activating inert N₂ molecules. For example, Zhao and Chen selected defective BN monolayer with B monovacancy as the anchoring material of single transition metal atoms for electrochemical N₂ fixation [110]. The DFT computations revealed that a single-Mo atom can be stably anchored by the unsaturated N atoms around the B vacancy in the BN monolayer, ensuring the structural stability. Confirmed by the theoretical calculations, the Mo-embedded BN nanosheet exhibited excellent catalytic activity toward NRR following the enzymatic mechanism with low overpotential of 0.19 V, which could be attributed to the facilitated chemisorption and activation of inert N₂ molecules, a selective stabilization of N₂H* and destabilization of NH₂* species.

Recently, several catalytic activity investigations by combination of experiments and theoretical calculations have been reported to confirm the potential of single-atom catalysts for the electrochemical conversion of N₂ into NH₃. For example, Wang et al. prepared atomic-level Au catalysts anchored on carbon nitride (Au/C₃N₄) with uniform dispersion evidenced by energy dispersive X-ray (EDX) spectroscopy elemental mappings and high-angle annular dark-field scanning transmission electron microscope (HAADF-STEM) characterizations (Fig. 11a–c) [115]. As-synthesized Au/C₃N₄ possessed excellent NRR catalytic activity with a Faradaic efficiency of 11.1% at −0.10 V vs RHE, outperforming the Au nanoparticles dispersed on C₃N₄. The computational studies demonstrated that the reduction of N₂ to NH₃ over the Au/C₃N₄ catalysts followed the favorable alternating mechanism with low Gibbs' free energies of the rate-determining step (1.33 eV), and the excellent catalytic performance might originate from the charge transfer between the Au atoms and the g-C₃N₄, enabling enhanced interaction with intermediates. However, the lack of ¹⁵N₂ isotopic experiments made it difficult to completely exclude the contribution of N sources in g-C₃N₄ to the produced NH₃ [115]. In another case, Geng and coworkers explored the electrocatalytic NRR activity of single-Ru atom catalysts supported on nitrogen-doped carbon (Ru/N-C) synthesized via the pyrolysis of Ru-containing derivative of zeolitic imidazolate frameworks (ZIF-8) (Fig. 11d) [116]. Notably, the Ru/N-C exhibited superior catalytic activity toward N₂ electrochemical reduction with high Faradaic efficiency of 29.6% and significant NH₃ yield rate of 120.9 μg h^{−1} mg^{−1} at −0.2 V vs RHE, resulting from the favorable chemical adsorption of N₂ and the promotion of subsequent N₂ dissociation serving as the rate-limiting step of the distal pathway. Similarly, Tao et al. also investigated the electrochemical N₂ fixation of sin-

gle-Ru atoms anchored on N-doped porous carbon (Ru@NC) but with the addition of ZrO₂ (Ru@ZrO₂/NC) to suppress the competitive HER [117]. A highest NH₃ yield rate of up to 3.665 mg h^{−1} mg^{−1}_{Ru} was obtained by the utilization of Ru@NC catalysts while the significantly improved Faradaic efficiency was achieved by the Ru@ZrO₂/NC with the help of ZrO₂ (Fig. 11e–f). The DFT calculations indicated that the Ru@NC₂ sites (i.e., single-Ru atom coordinated by one N atom and two C atoms) were the origin of the boosted NH₃ production rate due to the favorable N₂ adsorption and reduced Gibbs' free energy for potential-determining step of the NRR, and the Ru@Zr₃₂O₆₃ sites (i.e., single-Ru atom at O-vacancy sites in reduced ZrO₂) with O vacancies contributed to the improved NRR/HER selectivity owing to the suppressed H adsorption (Fig. 11g).

Metal-free materials

As the promising alternatives of metal-based catalysts, metal-free materials have attracted tremendous interest for a range of electrochemical reaction processes due to their economic viability, environment-friendly and non-corrosive nature, and unique physicochemical properties [118]. Particularly, carbon-based materials have emerged as efficient electrocatalysts with superior activity and stability owing to the excellent electrical conductivity and large specific surface area [119]. Furthermore, their catalytic activity can be significantly enhanced via the doping of heteroatoms for tuning the electronic structure and creating more defects [120]. Specifically, the introduction of heteroatoms with different electronegativity can induce charge transfer in carbon materials, promoting the reactant adsorption on electron-deficient sites [121]. For instance, Yu et al. proposed to use boron-doped graphene as an efficient carbon-based catalysts for catalyzing the reduction of N₂ to NH₃ at ambient conditions and investigated the effect of electron density redistribution caused by boron doping on the NRR catalytic activity (Fig. 12a) [122]. In comparison with undoped graphene (G), all the boron-doped graphene samples exhibited a better catalytic performance since the positively charged B-doping sites possessed strong binding capability of Lewis base (N₂) while prohibiting the adsorption of Lewis acid (H⁺), leading to the promotion of NRR Faradaic efficiency. Among three B-doped graphene samples with different fractions of various B-doped structures (Fig. 12b), the BG-1 (synthesized by thermal reduction in H₃BO₃ and graphene oxide with the mass ratios of 5:1) with the most significant percentage of BC₃ (a boron atom replaces a carbon atom in graphene framework) showed the highest NH₃ yield rate of 9.8 μg h^{−1} cm^{−2} and Faradaic efficiency of 10.8% at −0.5 V (Fig. 12c), indicating the BC₃ served as the most active sites for electrocatalytic NRR. The first-principle calculations suggested that the BC₃ possessed appropriate nitrogen-binding energies (0.01 eV) and the lowest reaction energy barrier (0.43 eV) of the limiting step in the distal pathway resulting in enhanced N₂ fixation, which was consistent with the results of experimental observations. Apart from the heteroatom doping, the construction of unique nanostructure can also bring positive effect on the electroreduction of N₂ molecules. For instance, Song et al. developed N-doped carbon nanospikes (CNS) consisting of multiple carbon layers ending in a sharp tip as the physical catalyst

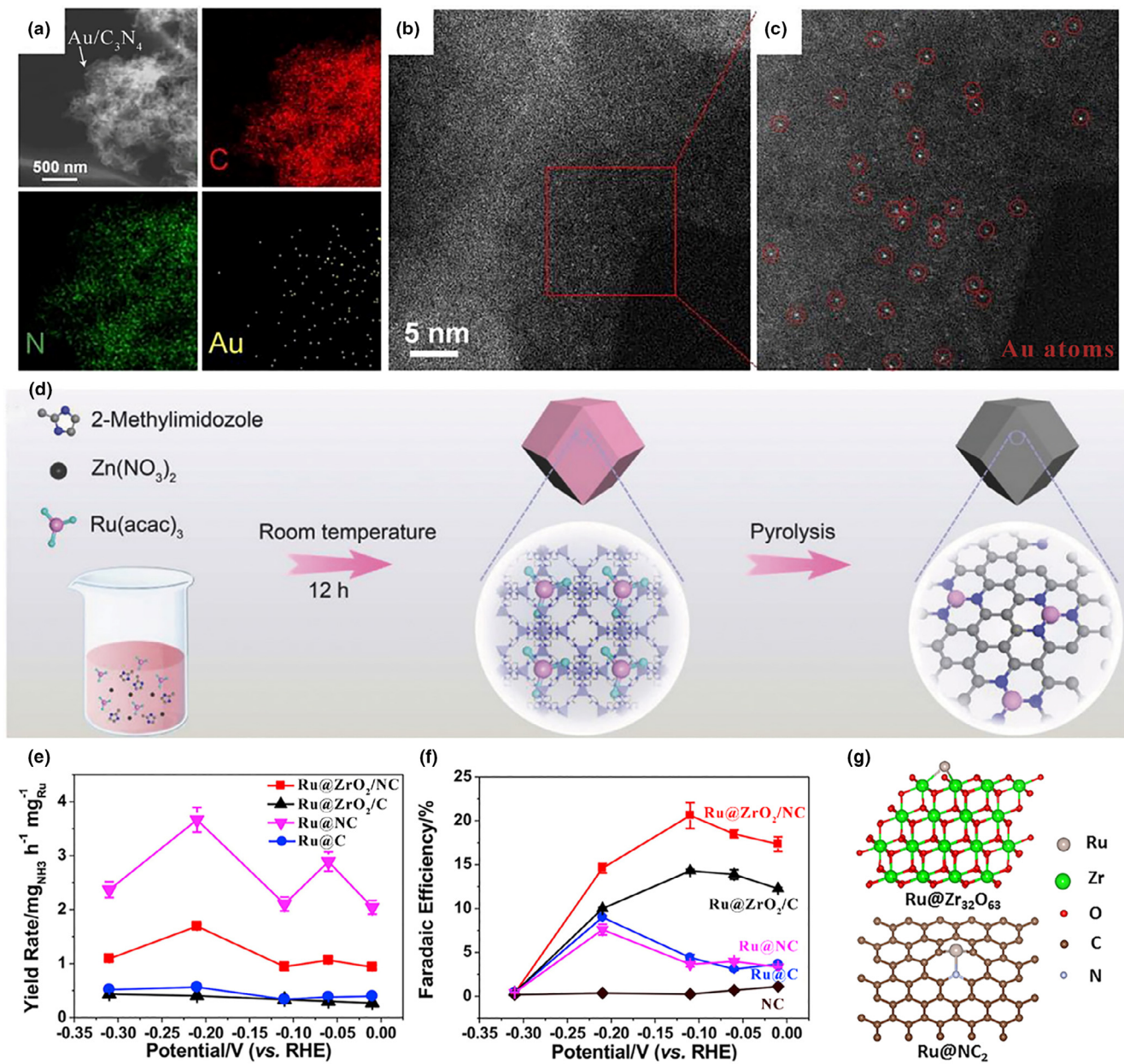
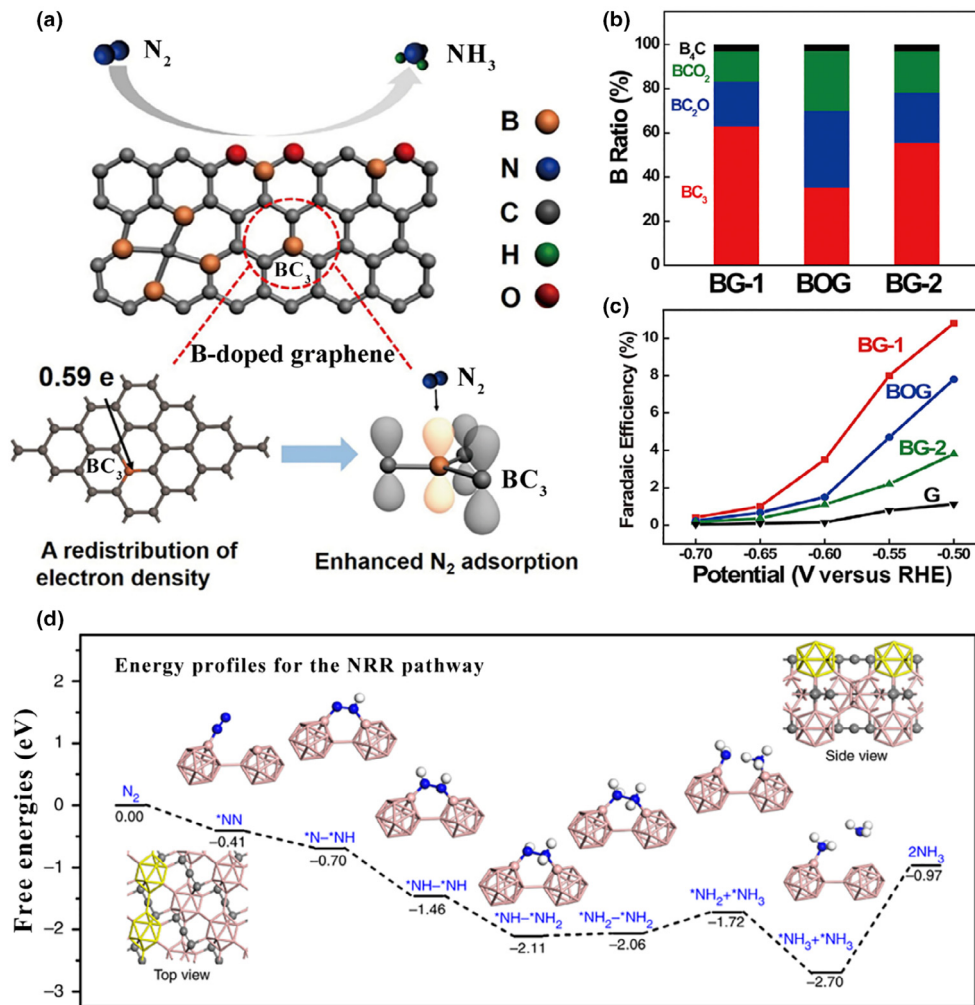


FIGURE 11

(a) Energy dispersive X-ray (EDX) spectroscopy elemental mapping results of Au/C₃N₄. (b, c) High-angle annular dark-field scanning transmission electron microscope (HAADF-STEM) images of Au/C₃N₄. Reproduced from Ref. [115] with permission from Elsevier. (d) Scheme of the synthetic procedure for single-Ru atom catalysts supported on nitrogen-doped carbon (Ru/N-C). Reproduced from Ref. [116] with permission from WILEY-VCH. (e) NH₃ yield rate and (f) Faradaic efficiency of single-Ru atoms anchored on N-doped porous carbon (Ru@NC), single-Ru atoms anchored on porous carbon (Ru@C), single-Ru atoms anchored on N-doped porous carbon with the addition of ZrO₂ (Ru@ZrO₂/NC), single-Ru atoms anchored on porous carbon with the addition of ZrO₂ (Ru@ZrO₂/C) at different applied potentials. (g) Calculation models for Ru@Zr₃₂O₆₃ (single-Ru atom at O-vacancy sites in reduced ZrO₂) and Ru@NC₂ (single-Ru atom coordinated by one N atom and two C atoms). Reproduced from Ref. [117] with permission from Elsevier.

for electrochemically reducing N₂ gas to NH₃ [123]. In contrast to oxygen plasma-etched (O-etched) CNS with sharp tip etched away, the pristine CNS showed a better NRR performance with a maximum NH₃ yield rate of 97.18 µg h⁻¹ cm⁻² and significant Faradaic efficiency of 11.56% at -1.19 V primarily because of the strong electric fields on the sharp tips, leading to the increased reagent concentration and thus facilitating N₂ electroreduction. Also, control experiments between various electrolytes, including LiClO₄, NaClO₄, and KClO₄, were carried out to evaluate the role

of electrolyte counterions. It turned out that the highest catalytic activity can be achieved in the presence of Li⁺ with the smallest cation size, which can be attributed to the increased electric field arising from the reduced counterion size and the relatively strong interaction between Li⁺ cations and N₂ molecules providing high concentrations of N₂ on the catalyst surface [123]. In addition to the carbon-based materials, other metal-free catalysts, such as boron carbide (B₄C) nanosheet, also exhibited excellent NRR activity [124]. The B₄C nanosheet could achieve a high NH₃

**FIGURE 12**

(a) Schematic illustration of NRR over B-doped graphene. (b) Percentages of different B doping configurations in three B-doped graphene samples. (c) The Faradaic efficiency values of BG-1 (synthesized by thermal reduction in H_3BO_3 and graphene oxide with the mass ratios of 5:1 in H_2/Ar gas), BOG (synthesized by thermal reduction in H_3BO_3 and graphene oxide with the mass ratios of 5:1 in Ar gas), BG-2 (synthesized by thermal reduction in H_3BO_3 and graphene oxide with the mass ratios of 1:10) and G (undoped graphene) at different applied potentials. Reproduced from Ref. [122] with permission from Elsevier. (d) Density functional theory (DFT) computed energy profiles for the electrocatalytic NRR processes following an alternating pathway on the boron carbide (B_4C) (110) surface. Reproduced from Ref. [124] with permission from the Nature Publishing Group.

production rate of $26.57 \mu\text{g h}^{-1} \text{ mg}^{-1}$ and a Faradaic efficiency of 15.95% at -0.75 V vs RHE, following an alternating pathway with the $^*\text{NH}_2-\text{NH}_2 \rightarrow ^*\text{NH}_2-\text{NH}_3$ reaction being the rate-limiting step (Fig. 12d), revealed by the DFT calculations.

Based on the above discussion, a NRR activity summary of these different electrocatalysts performing at ambient conditions is given in Table 2.

Summary and perspectives

In this review, effective material design strategies for improving the apparent activity or intrinsic activity of NRR electrocatalysts have been provided. On the basis of strategies for rationally tuning the catalyst activity, recent advances in emerging NRR electrocatalysts, including noble metal-based materials, transition metal-based materials, single-metal-atom catalysts, and metal-free materials operating at ambient conditions, are systematically summarized and the NRR performance of different catalysts are compared in Fig. 13. Although enormous progress has been

made in the optimization of reaction conditions enabling ammonia synthesis at room temperature and atmospheric pressure with the supply of nitrogen and water as proton source, most of the existing electrochemical NRR systems still suffer from high overpotential and low ammonia yield, as well as low Faradaic efficiency caused by the competing HER side reaction. To achieve electrocatalytic NRR close to the practical use, the following aspects are required to be considered:

- (1) Combination of theory and experiment for NRR. Theoretical calculations and computational studies have been utilized as powerful tools to predict the catalytic activity of potential catalysts and to reveal the possible reaction mechanism. Specifically, the adsorption free energy of reactants, the feasible reaction pathway demanding the least energy input, the energy barriers of corresponding rate-limiting steps and the required overpotential for driving the electrochemical reaction can be obtained on the

TABLE 2

Summary of recently reported NRR electrocatalysts.

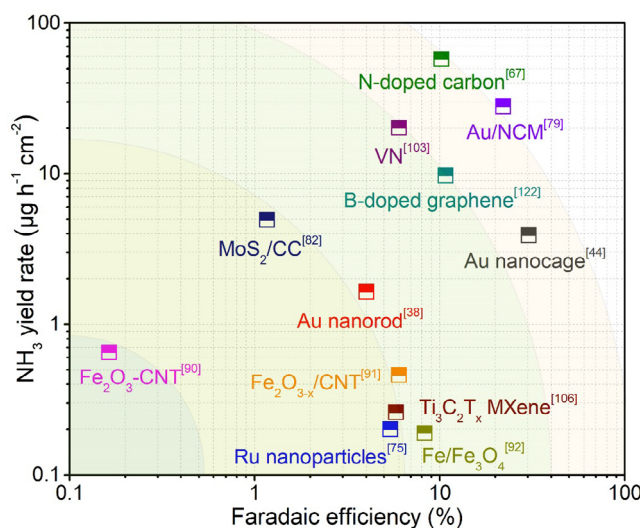
	Catalyst	Electrolyte	NH ₃ yield rate	Faradaic efficiency (%)	Potential (V vs RHE)	Ref.
Noble metal-based materials	Au nanorod	0.1 M KOH	1.648 µg h ⁻¹ cm ⁻²	4	-0.2	[38]
	Au nanocage	0.5 M LiClO ₄	3.9 µg h ⁻¹ cm ⁻²	30.2	-0.4	[44]
	Au flower	0.1 M HCl	25.57 µg h ⁻¹ mg ⁻¹	6.05	-0.2	[76]
	Ru nanoparticles	0.01 M HCl	~0.2 µg h ⁻¹ cm ⁻²	5.4	0.01	[75]
	Pd/C	0.1 M PBS	4.5 µg h ⁻¹ mg ⁻¹	8.2	0.1	[22]
	Rh nanosheet	0.1 M KOH	23.88 µg h ⁻¹ mg ⁻¹	0.217	-0.2	[78]
	Au/NCM	0.1 M HCl	~28 µg h ⁻¹ cm ⁻²	22	-0.1	[79]
	Au/CeO _x -RGO	0.1 M HCl	8.3 µg h ⁻¹ mg ⁻¹	10.1	-0.2	[80]
	Au/TiO ₂	0.1 M HCl	21.4 µg h ⁻¹ mg ⁻¹	8.11	-0.2	[125]
	Pd _{0.2} Cu _{0.8} /RGO	0.1 M KOH	2.8 µg h ⁻¹ mg ⁻¹	<1	-0.2	[81]
Non-noble metal-based materials	Fe ₂ O ₃ -CNT	diluted KHCO ₃	0.22 µg h ⁻¹ cm ⁻²	<0.15	-0.2 V vs Ag/AgCl	[89]
	30% Fe ₂ O ₃ -CNT	0.5 M KOH	0.65 µg h ⁻¹ cm ⁻²	0.164	-0.2 V vs Ag/AgCl	[90]
	Fe ₂ O _{3-x} /CNT	0.10 M KOH	0.46 µg h ⁻¹ cm ⁻²	6.0	-0.9 V vs Ag/AgCl	[91]
	Fe/Fe ₃ O ₄	0.1 M PBS	0.19 µg h ⁻¹ cm ⁻²	8.29	-0.3	[92]
	Fe	ionic liquids	0.29 µg h ⁻¹ cm ⁻²	60	-0.8 V vs NHE	[94]
	Fe ₃ O ₄ /Ti	0.1 M Na ₂ SO ₄	3.43 µg h ⁻¹ cm ⁻²	2.6	-0.4	[126]
	Cr ₂ O ₃	0.1 M Na ₂ SO ₄	~14 µg h ⁻¹ mg ⁻¹	6.78	-0.9	[85]
	MoO ₃	0.1 M HCl	29.43 µg h ⁻¹ mg ⁻¹	1.9	-0.3	[86]
	Nb ₂ O ₅	0.1 M HCl	43.6 µg h ⁻¹ mg ⁻¹	9.26	-0.55	[87]
	MoS ₂ /CC	0.1 M Na ₂ SO ₄	4.94 µg h ⁻¹ cm ⁻²	1.17	-0.5	[82]
	MoS ₂	0.1 M Na ₂ SO ₄	29.28 µg h ⁻¹ mg ⁻¹	8.34	-0.4	[83]
	CoP	1.0 M KOH	2.485 µg h ⁻¹ mg ⁻¹	7.36	0	[84]
	MoN/CC	0.1 M HCl	18.42 µg h ⁻¹ mg ⁻¹	1.15	-0.3	[99]
	Mo ₂ N	0.1 M HCl	78.4 µg h ⁻¹ mg ⁻¹	4.5	-0.3	[100]
	VN/Ti	0.1 M HCl	5.14 µg h ⁻¹ cm ⁻²	2.25	-0.5	[101]
	VN	0.05 M H ₂ SO ₄	20.2 µg h ⁻¹ cm ⁻²	6	-0.1	[103]
	Mo ₂ C/C	0.5 M Li ₂ SO ₄	11.3 µg h ⁻¹ mg ⁻¹	1.1	-0.3	[20]
	Ti ₃ C ₂ T _x MXene	N.A.	0.26 µg h ⁻¹ cm ⁻²	5.78	-0.2	[106]
Single-metal atom catalysts	Bi ₄ V ₂ O ₁₁ /CeO ₂	0.1 M HCl	23.21 µg h ⁻¹ mg ⁻¹	10.16	-0.2	[57]
	Au/C ₃ N ₄	5 mM H ₂ SO ₄	1.3 mg h ⁻¹ mg _{Au} ⁻¹	11.1	-0.1	[115]
	Ru/N-C	0.05 M H ₂ SO ₄	120.9 µg h ⁻¹ mg ⁻¹	29.6	-0.2	[116]
	Ru@ZrO ₂ /NC	0.1 M HCl	~1 mg h ⁻¹ mg _{Ru} ⁻¹	21	-0.11	[117]
Metal-free materials	NPC	0.05 M H ₂ SO ₄	23.8 µg h ⁻¹ mg ⁻¹	1.42	-0.9	[66]
	N-doped carbon	0.1 M KOH	57.8 µg h ⁻¹ cm ⁻²	10.2	-0.3	[67]
	PCN	0.1 M HCl	8.09 µg h ⁻¹ mg ⁻¹	11.59	-0.2	[58]
	B-doped graphene	0.05 M H ₂ SO ₄	9.8 µg h ⁻¹ cm ⁻²	10.8	-0.5	[122]
	CNS	0.25 M LiClO ₄	97.18 µg h ⁻¹ cm ⁻²	11.56	-1.19	[123]
	B ₄ C	0.1 M HCl	26.57 µg h ⁻¹ mg ⁻¹	15.95	-0.75	[124]

RHE: reversible hydrogen electrode; NHE: normal hydrogen electrode.

basis of theoretical investigations. Nevertheless, most of the theoretical studies are based on the simplified models at idealized conditions ignoring the decisive factors of electrochemical system (e.g., temperature, pH, mass transportation rate, proton supply, N₂ solubility, and the counterion effect), not to mention the surface reconstruction of catalysts during the practical reaction process. Therefore, theoretical calculations alone are not sufficient to reveal the catalytic behavior of catalysts, indicating the necessity of combining theoretical methods and experimental observations for the better understanding of catalytic reaction process under actual operating conditions.

(2) Selection of appropriate NRR catalysts. Among the reported NRR electrocatalysts so far, noble metal-based materials usually exhibit superior catalytic activity, whereas the high cost and limited resources hinder their practical applications. In terms of transition metal-based materials, Fe-based materials have been confirmed by

extensive investigations on their NRR catalytic performance but mainly focusing on iron oxide catalysts with a relatively poor stability under much negative potentials. Other Fe-based materials, including chalcogenides, carbides, and phosphides, might deserve to be further explored. In addition, in spite of a series of theoretical investigations demonstrating the potential of transition metal nitrides as NRR catalysts, the experimentally investigated nitride catalysts are still limited probably due to the possibility of N vacancy poisoning and catalyst decomposition during the reaction process, indicating that the construction of more efficient and stable nitrides in appropriate reaction system is important for achieving excellent NRR performance. Single-atom catalysts, as the promising NRR catalysts, need to be further investigated to broaden the range of dispersed metal atoms from noble metals to transition metals. In addition, metal-organic frameworks (MOF) or MOF-derived materials possessing highly porous structures and multiple catalytic active sites

**FIGURE 13**

An NRR performance map of different catalysts in terms of the NH₃ yield rate and the Faradaic efficiency. (NCM: nitrogen-doped nanoporous carbon membranes; CC: carbon cloth; CNT: carbon nanotube; Fe₂O_{3-x}: Fe₂O₃-containing oxygen vacancies).

are supposed to have promising application in electrochemical nitrogen-to-ammonia conversion.

(3) Rational design of efficient NRR catalysts. In order to further boost the electrocatalytic NRR, various material design strategies can be applied for improving the apparent activity or intrinsic activity of catalysts. Specifically, regulation of surface facets with favorable atomic arrangement and coordination can expose abundant active sites to capture N₂ molecules and break the triple bond of N₂. Optimization of the size and morphology of NRR electrocatalysts can create favorable coordination sites, which may influence the binding strength of reactants or key intermediates, such as the adsorption of N₂ or the desorption of *NH₂. In addition, the vacancy engineering, such as creating oxygen vacancies in oxide catalysts, can promote the cleavage of N≡N triple bond, since positively charged oxygen vacancies can trap metastable electrons, which may be transferred into an antibonding orbital of adsorbed N₂ molecules. Besides, heteroatom doping can modify the electronic structures and lower the absorption free energy toward N₂ molecules for improved NRR electrocatalytic activity. Although the strain engineering strategy has not been employed in the field of NRR, the modulation of the surface atomic spacing and the atomic bond length induced by strain engineering can be a promising strategy to alter the electronic structure, thus promoting the electrochemical NRR.

(4) Optimization of the electrolyte. Selection of suitable electrolyte holds the key to enhancing the efficiency and selectivity of the NRR reaction system. Confirmed by both theoretical analysis and experimental studies, limiting the proton availability in electrolyte can effectively suppress the HER and improve NRR selectivity. However, the utilization of the electrolyte of deficient proton supply

might reduce the ammonia yield rate primarily because certain quantities of protons are required to enable the N₂ hydrogenation for NH₃ production, demonstrating the importance of balancing the NRR selectivity and the ammonia yield rate with an appropriate proton supply in electrolyte. In addition, the choice of counterion in electrolyte might also have an impact on the nitrogen reduction. For example, compared with other counterions, Li⁺ possesses stronger interactions with N₂ molecules due to the favorable N₂-binding energy [123].

(5) Utilization of *in situ*/operando characterizations. Identification of the catalytic mechanism and the reaction process is crucial for the rational design of NRR catalysts, which mainly relies on the theoretical investigations. However, the pristine catalysts usually experience transformations of the surface structure, the element valence state and the exposed active sites, which are difficult to be predicted accurately by the theoretical calculations. For this reason, the development of *in situ*/operando characterizations to probe the catalyst surface transformation and adsorbed intermediates is of great significance to reveal the real catalytic process and reaction pathway under the operating conditions, providing a better understanding of NRR mechanism. Besides, the utilization of *in situ*/operando characterizations can scrutinize the catalytic active sites on the catalyst surface, offering a guide to the development of efficient NRR electrocatalysts.

In summary, recent advances in the development of heterogeneous NRR catalysts have validated the potentials of electrochemical nitrogen-to-ammonia conversion operating at ambient conditions. Nevertheless, the relatively low ammonia yield and conversion efficiency are expected to be further improved to satisfy the demand for their practical applications. In this regard, a rational design of efficient NRR catalysts on the basis of theoretical calculations and experimental investigations, together with the establishment of reliable ammonia detection method and the use of advanced characterization techniques are believed to further promote the advancement of electrocatalytic NRR as a green and more sustainable process with low energy consumption.

Acknowledgments

We acknowledge the financial support from the National Natural Science Foundation of China for Excellent Young Scholars (Grant No. 51722207), 973 program of China (Grant No. 2015CB932500) and the Tsinghua University Initiative Scientific Research Program (Grant No. 20151080367).

References

- [1] J. Deng et al., Joule 2 (2018) 846–856.
- [2] S.L. Foster et al., Nat. Catal. 1 (2018) 490–500.
- [3] M.A. Shipman, M.D. Symes, Catal. Today 286 (2017) 57–68.
- [4] J.M. McEnaney et al., Environ. Sci. 10 (2017) 1621–1630.
- [5] Y. Tanabe, Y. Nishibayashi, Coord. Chem. Rev. 257 (2013) 2551–2564.
- [6] S. Licht et al., Science 345 (2014) 637–640.
- [7] T. Oshikiri et al., Angew. Chem. Int. Ed. 128 (2016) 4010–4014.
- [8] M. Kitano et al., Nat. Chem. 4 (2012) 934.
- [9] M.K. Chan et al., Science 260 (1993) 792.
- [10] B.M. Hoffman et al., Chem. Rev. 114 (2014) 4041–4062.

- [11] T. Spatzl et al., *Science* 334 (2011) 940.
- [12] K.M. Lancaster et al., *Science* 334 (2011) 974.
- [13] K.C. Macleod, P.L. Holland, *Nat. Chem.* 5 (2013) 559–565.
- [14] H.P. Jia, E.A. Quadrelli, *Chem. Soc. Rev.* 43 (2014) 547–564.
- [15] J. Rittle, J.C. Peters, *J. Am. Chem. Soc.* 138 (2016) 4243–4248.
- [16] C. Guo et al., *Environ. Sci.* 11 (2018) 45–56.
- [17] Y. Zhao et al., *Adv. Mater.* 29 (2017) 1703828.
- [18] G. Zhao et al., *J. Mater. Chem. A* 5 (2017) 21625–21649.
- [19] X. Cui et al., *Adv. Energy Mater.* 8 (2018) 1800369.
- [20] H. Cheng et al., *Adv. Mater.* 30 (2018) 1803694.
- [21] C.J.M. van der Ham et al., *Chem. Soc. Rev.* 43 (2014) 5183–5191.
- [22] J. Wang et al., *Nat. Commun.* 9 (2018) 1975.
- [23] J.H. Montoya et al., *ChemSusChem* 8 (2015) 2180–2186.
- [24] A.R. Singh et al., *ACS Catal.* 7 (2017) 706–709.
- [25] Z.W. Seh et al., *Science* 355 (2017) eaad4998.
- [26] G.-F. Chen et al., *Small Methods* (2018) 1800337, <https://doi.org/10.1002/smtd.201800337>.
- [27] E. Skúlason et al., *Phys. Chem. Chem. Phys.* 14 (2012) 1235–1245.
- [28] C.C. McCrory et al., *J. Am. Chem. Soc.* 137 (2015) 4347–4357.
- [29] Z.F. Huang et al., *Adv. Energy Mater.* 7 (2017) 1700544.
- [30] Y. Yang et al., *Chem* 4 (2018) 2054–2083.
- [31] J.W. Hong et al., *Chem. Asian J.* 11 (2016) 2224–2239.
- [32] M. Shao et al., *Chem. Rev.* 116 (2016) 3594–3657.
- [33] W.J. Durand et al., *Surf. Sci.* 605 (2011) 1354–1359.
- [34] F.S. Roberts et al., *Angew. Chem. Int. Ed.* 54 (2015) 5179–5182.
- [35] Z.L. Wang et al., *Nano Today* 11 (2016) 373–391.
- [36] W. Luo et al., *ACS Catal.* 6 (2015) 219–229.
- [37] D. Yang et al., *J. Mater. Chem. A* 5 (2017) 18967–18971.
- [38] D. Bao et al., *Adv. Mater.* 29 (2017) 1604799.
- [39] H. Mistry et al., *Nat. Rev. Mater.* 1 (2016) 16009.
- [40] R. Reske et al., *J. Am. Chem. Soc.* 136 (2014) 6978–6986.
- [41] W. Xiao et al., *ACS Catal.* 8 (2018) 3237–3256.
- [42] J. Qian et al., *Mater. Today* 21 (2018) 834–844.
- [43] J. Kibsgaard et al., *Nat. Mater.* 11 (2012) 963–969.
- [44] M. Nazemi et al., *Nano Energy* 49 (2018) 316–323.
- [45] M. Nazemi, M.A. El-Sayed, *J. Phys. Chem. Lett.* 9 (2018) 5160–5166.
- [46] Z. Cai et al., *Adv. Energy Mater.* 8 (2018) 1701694.
- [47] A.Y. Lu et al., *Small* 12 (2016) 5530–5537.
- [48] Y. Sun et al., *Chem. Commun.* 52 (2016) 14266–14269.
- [49] Y. Liu et al., *J. Am. Chem. Soc.* 136 (2014) 15670–15675.
- [50] S. Dou et al., *Small Methods* (2018) 1800211, <https://doi.org/10.1002/smtd.201800211>.
- [51] S. Gao et al., *Nat. Commun.* 8 (2017) 14503.
- [52] J. Kim et al., *J. Am. Chem. Soc.* 136 (2014) 14646–14649.
- [53] T. Ling et al., *Nat. Commun.* 7 (2016) 12876.
- [54] X. Wang et al., *Adv. Mater.* 29 (2017) 1603617.
- [55] H. Li et al., *J. Am. Chem. Soc.* 137 (2015) 6393–6399.
- [56] H. Hirakawa et al., *J. Am. Chem. Soc.* 139 (2017) 10929–10936.
- [57] C. Lv et al., *Angew. Chem. Int. Ed.* 130 (2018) 6181–6184.
- [58] C. Lv et al., *Angew. Chem. Int. Ed.* 57 (2018) 10246–10250.
- [59] J. Huang et al., *Adv. Mater.* 30 (2018) 1705045.
- [60] W. Xiao et al., *Adv. Energy Mater.* 7 (2017) 1602086.
- [61] X. Du et al., *Angew. Chem. Int. Ed.* (2018), <https://doi.org/10.1002/ange.201810104>.
- [62] H. Jin et al., *Chem. Rev.* 118 (2018) 6337–6408.
- [63] J. Xie et al., *J. Am. Chem. Soc.* 135 (2013) 17881–17888.
- [64] D.Y. Wang et al., *J. Am. Chem. Soc.* 137 (2015) 1587–1592.
- [65] J. Li et al., *Adv. Funct. Mater.* 26 (2016) 6785–6796.
- [66] Y. Liu et al., *ACS Catal.* 8 (2018) 1186–1191.
- [67] S. Mukherjee et al., *Nano Energy* 48 (2018) 217–226.
- [68] M. Luo, S. Guo, *Nat. Rev. Mater.* 2 (2017) 17059.
- [69] P. Strasser et al., *Nat. Chem.* 2 (2010) 454–460.
- [70] D. Voiry et al., *Nat. Mater.* 12 (2013) 850–855.
- [71] H. Wang et al., *Science* 354 (2016) 1031.
- [72] T. Ling et al., *Nat. Commun.* 8 (2017) 1509.
- [73] H.L. Liu et al., *Chem. Soc. Rev.* 44 (2015) 3056–3078.
- [74] J. Gu et al., *Chem. Soc. Rev.* 41 (2012) 8050–8065.
- [75] D. Wang et al., *ChemSusChem* 11 (2018) 3416–3422.
- [76] Z. Wang et al., *ChemSusChem* 11 (2018) 3480–3485.
- [77] Y. Jiang et al., *Nano Res.* 9 (2016) 849–856.
- [78] H.-M. Liu et al., *J. Mater. Chem. A* 6 (2018) 3211–3217.
- [79] H. Wang et al., *Angew. Chem. Int. Ed.* 57 (2018) 12360–12364.
- [80] S.J. Li et al., *Adv. Mater.* 29 (2017) 1700001.
- [81] M.M. Shi et al., *Adv. Energy Mater.* 8 (2018) 1800124.
- [82] L. Zhang et al., *Adv. Mater.* 30 (2018) 1800191.
- [83] X. Li et al., *Adv. Energy Mater.* 8 (2018) 1801357.
- [84] W. Guo et al., *Small Methods* 2 (2018) 1800204.
- [85] Y. Zhang et al., *ACS Catal.* 8 (2018) 8540–8544.
- [86] J. Han et al., *J. Mater. Chem. A* 6 (2018) 12974–12977.
- [87] J. Han et al., *Nano Energy* 52 (2018) 264–270.
- [88] M.T. Nguyen et al., *Phys. Chem. Chem. Phys.* 17 (2015) 14317–14322.
- [89] S. Chen et al., *Angew. Chem. Int. Ed.* 56 (2017) 2699–2703.
- [90] S. Chen et al., *ACS Sustain. Chem. Eng.* 5 (2017) 7393–7400.
- [91] X. Cui et al., *Chem. Eur. J.* 24 (2018) 1–9.
- [92] L. Hu et al., *ACS Catal.* 8 (2018) 9312–9319.
- [93] B.H.R. Suryanto et al., *ACS Energy Lett.* 3 (2018) 1219–1224.
- [94] F. Zhou et al., *Environ. Sci.* 10 (2017) 2516–2520.
- [95] Y. Abghouei, E. Skúlason, *J. Phys. Chem. C* 121 (2017) 6141–6151.
- [96] Y. Abghouei et al., *ACS Catal.* 6 (2015) 635–646.
- [97] Y. Abghouei, E. Skúlason, *Catal. Today* 286 (2017) 78–84.
- [98] Y. Abghouei, E. Skúlason, *Catal. Today* 286 (2017) 69–77.
- [99] L. Zhang et al., *ACS Sustain. Chem. Eng.* 6 (2018) 9550–9554.
- [100] X. Ren et al., *Chem. Commun.* 54 (2018) 8474–8477.
- [101] R. Zhang et al., *ACS Sustain. Chem. Eng.* 6 (2018) 9545–9549.
- [102] X. Zhang et al., *Chem. Commun.* 54 (2018) 5323–5325.
- [103] X. Yang et al., *J. Am. Chem. Soc.* 140 (2018) 13387–13391.
- [104] L.M. Azofra et al., *Environ. Sci.* 9 (2016) 2545–2549.
- [105] I. Matanovic, F.H. Garzon, *Phys. Chem. Chem. Phys.* 20 (2018) 14679–14687.
- [106] Y. Luo et al., *Joule* 3 (2018) 1–11.
- [107] C. Zhu et al., *Angew. Chem. Int. Ed.* 56 (2017) 13944–13960.
- [108] J. Su et al., *J. Mater. Chem. A* 6 (2018) 14025–14042.
- [109] X.F. Li et al., *J. Am. Chem. Soc.* 138 (2016) 8706–8709.
- [110] J. Zhao, Z. Chen, *J. Am. Chem. Soc.* 139 (2017) 12480–12487.
- [111] Z. Wei et al., *J. Mater. Chem. A* 6 (2018) 13790–13796.
- [112] L.M. Azofra et al., *Chem. Eur. J.* 23 (2017) 8275–8279.
- [113] C. Ling et al., *J. Phys. Chem. C* 122 (2018) 16842–16847.
- [114] C. Choi et al., *ACS Catal.* 8 (2018) 7517–7525.
- [115] X. Wang et al., *Sci. Bull.* 63 (2018) 1246–1253.
- [116] Z. Geng et al., *Adv. Mater.* 30 (2018) 1803498.
- [117] H. Tao et al., *Chem* 5 (2018) 1–11.
- [118] C.V.S. Kumar, V. Subramanian, *Phys. Chem. Chem. Phys.* 19 (2017) 15377–15387.
- [119] M. Tahir et al., *Nano Energy* 37 (2017) 136–157.
- [120] L. Zhang et al., *Small* 14 (2018) 1800235.
- [121] G. Wu et al., *Nano Energy* 29 (2016) 83–110.
- [122] X. Yu et al., *Joule* 2 (2018) 1610–1622.
- [123] Y. Song et al., *Sci. Adv.* 4 (2018) e1700336.
- [124] W. Qiu et al., *Nat. Commun.* 9 (2018) 3485.
- [125] M.M. Shi et al., *Adv. Mater.* 29 (2017) 1606550.
- [126] Q. Liu et al., *Nanoscale* 10 (2018) 14386–14389.